Study of multipolar effects in rare earth and actinide intermetallic compounds by μSR

2004 J. Phys.: Condens. Matter 16 S4639

(http://iopscience.iop.org/0953-8984/16/40/013)

INSTITUTE OF PHYSICS PUBLISHING JOURNAL OF PHYSICS: CONDENSED MATTER

J. Phys.: Condens. Matter **16** (2004) S4639–S4686 PII: S0953-8984(04)84857-4

Study of multipolar effects in rare earth and actinide intermetallic compounds by μSR

A Schenck[1] **and G Solt**[2]

[1] Institute for Particle Physics of ETH Zurich, 5232 Villigen PSI, Switzerland
[2] Paul Scherrer Institut, 5232 Villigen PSI, Switzerland

Received 6 April 2004
Published 24 September 2004
Online at stacks.iop.org/JPhysCM/16/S4639
doi:10.1088/0953-8984/16/40/013

Abstract

A review is presented of μSR measurements on CeB_6, $Ce_{1-x}La_xB_6$, CeAg, $PrCu_2$, HoB_2C_2, $DyPd_3S_4$ and UPd_3 which reveal multipolar, in particular quadrupolar, effects. μ^+ Knight shift data imply that the spin polarization of conduction electrons at the μ^+ may acquire an unusual temperature dependence and anisotropy in the presence of a non-spherical charge distribution of the f-electrons. This feature is also discussed theoretically. The interplay of dipolar magnetic and electric quadrupolar order is shown to possibly explain properties of the spontaneous fields at the μ^+ in the magnetically ordered state, as well as aspects of the μ^+ spin lattice relaxation. The possibility of magnetic-octupolar effects is briefly considered.

1. Introduction

Since the 1970s it has become increasingly recognized that the elastic, magnetic and structural properties of rare earth and actinide intermetallic compounds and oxides are affected by multipolar interactions in addition to the crystalline electric field acting on the 4f and 5f electrons [1]. Besides the well studied spin–spin exchange and superexchange mechanisms and the one-ion and two-ion magneto-elastic couplings, the two-ion electric quadrupolar and magnetic-octupolar interactions may have to be considered. While the latter are not yet experimentally demonstrated beyond doubt, quadrupolar interactions and quadrupolar ordering phenomena are observed in many compounds. The necessary condition is that the orbital angular momentum of the f-electron shell is not quenched and that the lowest lying levels of the CEF-split ground state multiplet (LSJ) involve a charge distribution which is not spherically symmetric and is characterized by non-zero components of the quadrupole moment tensor which may be written as

$$(Q_{ij})_{\Gamma\lambda} = \langle \Gamma\lambda | Q_{ij} | \Gamma\lambda \rangle$$

where $Q_{ij} = \frac{3Q}{2J(2J-1)}(J_iJ_j + J_jJ_i - \frac{2}{3}J(J+1)\delta_{ij})$ is the quadrupole operator. The constant Q is the (ionic) quadrupole moment and $|\Gamma\lambda\rangle$ is the λth eigenfunction of the Γth CEF level. In cubic

systems intrinsic non-zero quadrupole moments are not possible in singlet or Kramers-doublet ground states, but they are in triplet and quartet states and non-Kramers doublets. Quadrupole moments, or corresponding non-spherical charge distributions, can be induced, among others, by strain involving the strain susceptibility χ_μ, which for a singlet ground state shows a Van Vleck behaviour, in complete analogy to the magnetic susceptibility.

The bilinear quadrupole–quadrupole interaction of neighbouring f-electron ions can lead to ferro- or antiferroquadrupolar order, which, like in the case of magnetic order, is characterized by a propagation vector $\boldsymbol{q}_{\mathrm{Q}}$. Quadrupolar order represents a type of orbital order. In contrast to dipolar magnetic order, it is invariant under time reversal.

The onset of quadrupolar order is usually (but not always) accompanied by a structural change, leading to a lowering of the crystal symmetry (e.g. from cubic to tetragonal) and is sometimes viewed as a Jahn–Teller transition. It always leads to a lifting of the degeneracy, e.g. a quartet state splits into two doublets.

Via the strong LS coupling, as compared to the CEF splittings, of the f-electrons, magnetic and quadrupolar features are closely related, as particularly well reflected in the field induced magnetic order in the quadrupolar phase, which is observed in various compounds (e.g. in CeB_6 [2]).

The presence of quadrupolar interactions is revealed in many properties, such as specific heat, magnetization, magnetostriction, metamagnetism, elasticity, crystal structure, ultrasound absorption, etc, seen by many methods and techniques ranging from de Haas–van Alphen measurement to synchrotron x-ray scattering. It is not obvious, however, that μSR can also be a sensitive technique, since the positive muon is a magnetic probe that is essentially blind to the shape of the charge distribution on neighbouring atoms or ions. But, as will be demonstrated, μSR measurements have shown the powerful potential also to study quadrupole related effects in metallic compounds via the study of the contact hyperfine coupling to the conduction electrons, contributing to the μ^+ Knight shift, and through the spin–lattice-relaxation, induced possibly by fluctuating contact hyperfine fields in the paraquadrupolar phase. The compounds displaying quadrupolar related features in μSR measurements are up to now $PrCu_2$, CeB_6, $Ce_{0.75}La_{0.25}B_6$, CeAg, DyP_3S_4, HoB_2C_2 and UPd_3.

As pointed out before, magnetic octupolar ordering, although widely discussed, has not really materialized as yet in experiments. It is speculated that octupolar order may be present in phase IV of $Ce_{1-x}La_xB_6$ ($x = 0.25$–0.3) and in NpO_2 [3, 4].

Below we will provide some background information on the compounds listed above.

(1) $PrCu_2$. This orthorhombic compound is known to show an incommensurate, sinusoidally modulated magnetic structure below ∼50 mK [5] and ferroquadrupolar order below $T_{\mathrm{Q}} \sim 7.5$ K [6]. A phase diagram concerning the ferroquadrupolar order is displayed in figure 1. The ferroquadrupolar phase boundary depends strongly on along which axis the external field is applied. More recently a metamagnetic transition was also studied [7]. Both the metamagnetic transition and the antiferroquadrupolar transition could be quantitatively explained on the basis of the CEF Hamiltonian acting on the $^3H_4$ ground state multiplet of Pr^{3+} and quadrupole–quadrupole interaction terms applying a mean field approximation. Namely the term $K_{\mathrm{JT}}\langle O_{xy}\rangle O_{xy}$ is responsible for the ferroquadrupolar order below T_{Q} and the term $K_{\mathrm{M}}\langle O_2^2\rangle O_2^2$ switches its sign from negative to positive across the metamagnetic transition as a result of a rotation of the quadrupole moment O_2^2 [8]. K_{JT} and K_{M} are coupling parameters. The CEF interaction splits the $^3H_4$ multiplet into nine singlets. For $T > T_{\mathrm{Q}}$ the first excited state is about 6 K above the lowest level; for $T < T_{\mathrm{Q}}$ it is only about 3 K above the lowest level.

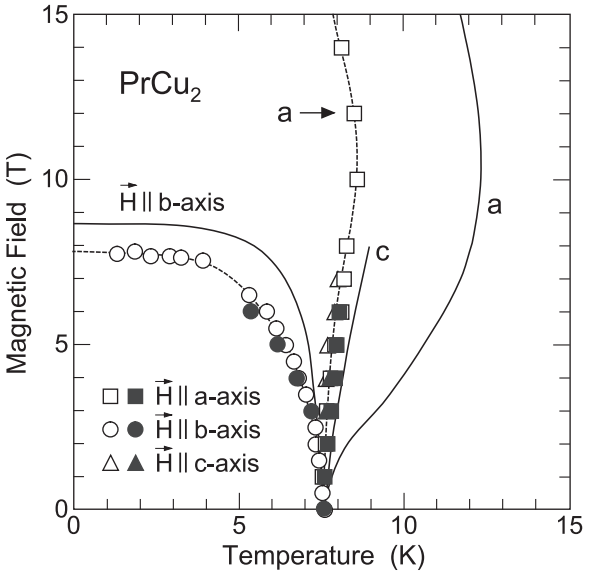

Figure 1. Phase diagram of $PrCu_2$ in the H–T plane showing the phase boundary to the ferroquadrupolar state and its dependence on the orientation of the applied field. The solid curves represent theoretical predictions (from [8]).

(2) CeB_6, $Ce_{1-x}La_xB_6$. Cubic CeB_6 is perhaps the best studied, but still controversially discussed compound showing antiferroquadrupolar order. The lowest level of the CEF split $^2F_{5/2}$ ground state multiplet is the Γ_8 quartet.

The phase diagram in the field–temperature plane is displayed in figure 2 [2]. In zero and small applied fields at the lowest temperatures one finds a rather complex modulated antiferromagnetic structure, phase III [9]. In higher field a single-$\boldsymbol{k}$ structure replaces the complex double-$\boldsymbol{k}$ structure [2]. Above a field of 2 T, T_N eventually becomes zero. The transition temperature T_Q to the antiferroquadrupolar phase II rises continuously with the applied field up to at least 16 T, implying that the quadrupolar phase is stabilized by the applied field. This is believed to originate from field induced octupolar moments [10]. The antiferroquadrupolar (AFQ) order has been observed directly by resonant x-ray scattering, allowing one to determine the temperature dependence of the AFQ order parameter in the presence of different magnetic fields [11].

When applying a field in phase II both neutron diffraction [2] and NMR measurements [12] reveal a field induced magnetic order. According to the neutron work this antiferromagnetic order appears to be of a simple G type with propagation vector $\boldsymbol{q} = (\frac{1}{2}\frac{1}{2}\frac{1}{2})$ that also describes the antiferroquadrupolar order. The NMR results were originally interpreted in terms of a triple-$\boldsymbol{q}$ structure [12]. This discrepancy gave rise to much discussion, but has recently been resolved by considering field induced magnetic octupolar moments of the 4f electron state and its associated hyperfine fields at the boron sites [10].

Replacing a fraction $x < 0.8$ of the Ce ions by La a more complex phase diagram appears, as shown in figure 3 for $x = 0.25$ [13]. A new phase IV shows up whose true nature is still not settled. The antiferroquadrupolar phase II can only be reached in applied fields exceeding ~0.6 T. The boundary between phase III and phase II again depends strongly on along which crystal axis the field is applied. On changing the La content to 0.3,

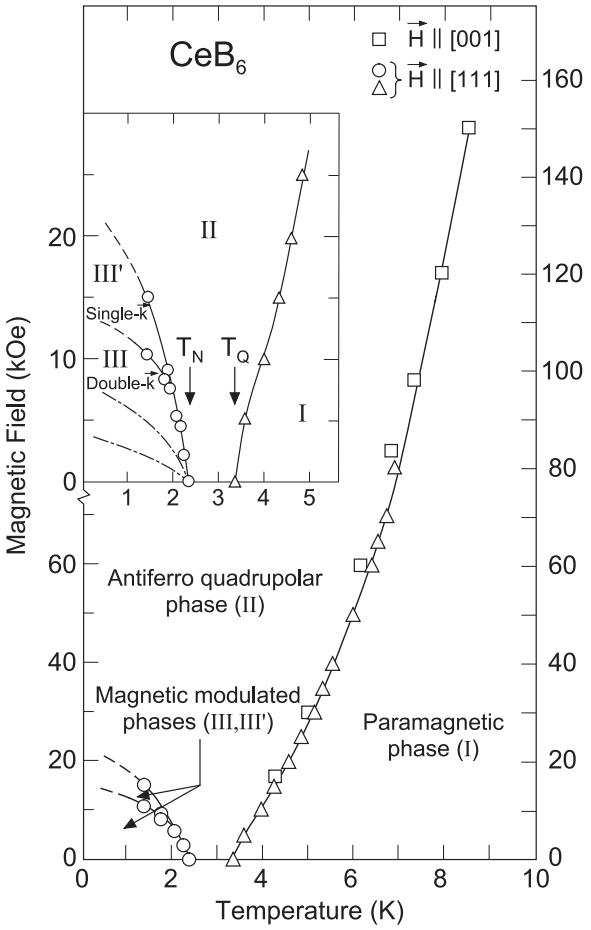

Figure 2. Phase diagram of CeB_6, showing the magnetic phase III, the antiferroquadrupolar phase II and the paramagnetic phase I. The magnetic phase displays a double-$\boldsymbol{k}$ antiferromagnetic structure (III) and a single-$\boldsymbol{k}$ structure at higher fields (III′). The phase boundary between III and II depends strongly on the orientation of the applied field (not shown), but not the boundary between II and I (from [2]).

the new phase IV extends down to 0 K for fields up to ∼0.7 T, pushing phase III up to fields >0.7 T [14]. Recent neutron diffraction work on $Ce_{0.75}La_{0.25}B_6$ seems to show in phase III the same magnetic structure as in phase III of CeB_6 [15]. This appears to be at variance with ZF-μSR data (see section 4). Kubo and Kuramoto [16, 3] propose an octupole ordering model for phase IV.

(3) *CeAg*. This cubic compound possesses ferromagnetic order below $T_c \simeq 5.5$ K and a structural phase transition, driven by ferroquadrupolar order, at $T_Q = 15$–16 K [1]. The latter changes the crystal structure from cubic to tetragonal with $(a/c) - 1 \simeq 1.9\%$ [17]. The ordered moment is probably oriented along the tetragonal axis [18]. Ce^{3+} is a Kramers ion; the ground state in the cubic phase is the Γ_8 quartet, as in CeB_6.

(4) *HoB_2C_2*. It is a tetragonal (space group $P4/mbm$) compound and is exceptional in that the antiferroquadrupolar order ($T_Q = 4.5$ K) develops inside the antiferromagnetic state ($T_N = 5.9$ K) [19]. The tetragonal CEF interaction splits the $^5I_8$ ground state multiplet

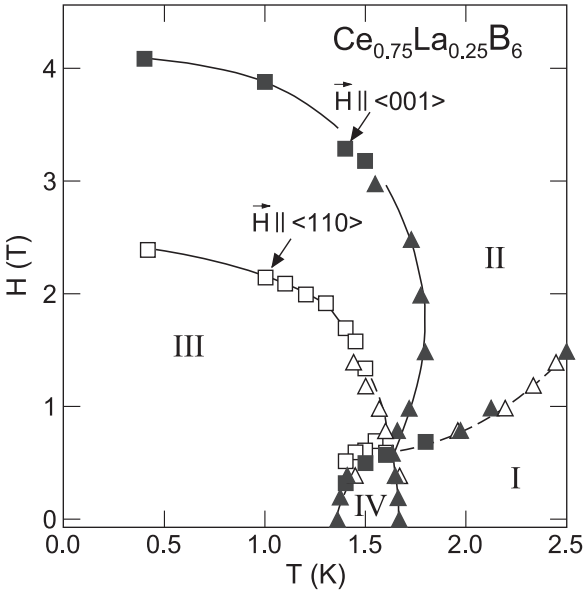

Figure 3. Magnetic and quadrupolar phase diagram of $Ce_{0.75}La_{0.25}B_6$. A new phase IV is observed. The phase boundary between III and II depends again on the orientation of the applied field (from [13]).

of Ho^{3+} into four doublets and nine singlets. The lowest level is presumably a pseudo triplet [20].

(5) *$DyPd_3S_4$*. This cubic compound with $NaPt_3O_4$-type crystal structure belongs to the rare earth palladium bronzes. It shows a transition to an antiferroquadrupolar order at $T_Q = 3.4$ K followed by two successive magnetic dipolar transitions at $T_{N_1} = 0.9$ K and $T_{N_2} = 0.7$ K [21, 22]. Neutron diffraction revealed the magnetic structure to be canted antiferromagnetic with different canting angles below T_{N_1} and T_{N_2}, respectively [22]. The cubic CEF splits the $^6H_{15/2}$ ground state multiplet of Dy^{3+} into two doublets and three quartets. The lowest level is expected to be an orbitally degenerate quartet or pseudo quartet (two nearly degenerate Kramers doublets). Inelastic neutron scattering results point to a splitting of the quartet state below T_Q, driven by the onset of quadrupolar order [22]. No lattice distortion is observed across T_Q [22].

(6) *UPd_3*. The double-hexagonal close-packed structure of UPd_3 leads to two different U sublattices with hexagonal and quasi-cubic local symmetry at the U sites, rendering the CEF splitting and the magnetic response of the two types of U^{4+} ions different. Various measurements showed the presence of three phase transitions at $T_0 = 7.6$ K, $T_1 = 6.8$ K and $T_2 = 4.4$ K [23]. A phase diagram in the field–temperature plane is shown in figure 4 for $\boldsymbol{H}_{ext} \parallel a$-axis [24]. Quite a different behaviour is found when $\boldsymbol{H}_{ext} \parallel c$-axis (not shown) [28]. Polarized neutron diffraction studies demonstrate the development of a periodic lattice distortion below T_0, with a doubling of the crystallographic unit cell, driven by the onset of antiferroquadrupolar order [24]. The transition at T_1 is likewise attributed to a change of the quadrupolar order parameter [25]. Definitive evidence for antiferroquadrupolar order is provided by the observation of resonant x-ray scattering from the aspherical charge distribution around the U ions [26]. Below T_0, the ordered quadrupole moments of $Q_{x^2-y^2}$-type are predominantly on the quasi-cubic sites: the unit

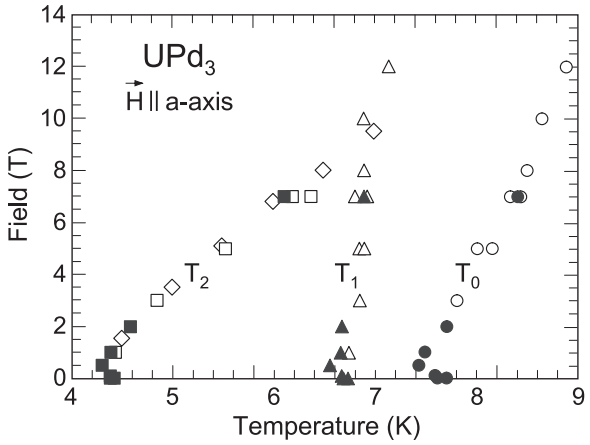

Figure 4. Phase diagram of UPd_3 showing the boundaries between the different antiferroquadrupolar phases (from [24]).

cell is orthorhombic with an antiphase stacking of the moments along the *c*-direction. Below T_1, a rotation and tilt of the quadrupoles is required to explain the x-ray and neutron results. The transition at T_2 is in part magnetic, involving tiny moments of $\sim 10^{-2}\mu_B$/U, and involves also a change of the antiferroquadrupolar order parameter. However, true long range magnetic order does not seem to be present [24, 25]. See also section 4.4.

As pointed out above, the quasi-cubic and hexagonal sublattices have different magnetic susceptibilities, $\overleftrightarrow{\chi}_{\rm hex}$. Polarized neutron diffraction measurements show that $\chi_{\rm cub}^{\perp C} \simeq (3\text{–}5)\chi_{\rm hex}^{\perp C}$ and $\chi_{\rm cub}^{\parallel C} \gg \chi_{\rm hex}^{\parallel C} \approx 0$ below 10 K [25, 27]. Therefore, below 10 K, the quasi-cubic sublattice provides the dominating contribution to the bulk susceptibility $\overleftrightarrow{\chi}_{\rm bulk}$.

The remainder of this paper is organized as follows. In section 2 we discuss the presence of quadrupolar effects in the μ^+ Knight shift. Section 3 provides a theoretical basis for the understanding of the effects presented in section 2. In section 4 the interplay of multipolar magnetic order and electric quadrupolar order, as observed in the experiments, is described. Section 5 discusses spin lattice relaxation data in relation to quadrupolar effects. The short section 6 addresses the suggestion that magnetic octupolar order in NpO_2 and in phase IV of $Ce_{1-x}La_xB_6$ ($x = 0.25$–0.3) could explain the presence of spontaneous magnetic fields at the μ^+. Finally in section 7 a summary and conclusions are given.

2. Quadrupolar effects reflected in the μ^+ Knight shift

2.1. Introduction

In the paramagnetic state of rare earth and actinide intermetallic compounds the μ^+ Knight shift K is predominantly related to the magnetic response of the rare earth or actinide constituents, expressed by the susceptibility tensor $\overleftrightarrow{\chi}$. Polarizing the f-electron moments by an external magnetic field leads to dipolar and contact-hyperfine fields at the μ^+ site, the latter induced by the f-electron moments via the RKKY interaction. We write [29]

$$K_i = (A_i^{\rm dip} + A_i^{\rm con})\chi_i + K_i^0 \tag{2.1}$$

where i refers to a symmetry axis of the crystal in question, which is usually also a principal axis of the susceptibility tensor $\overleftrightarrow{\chi}$. $A_i^{\rm dip}$ is the corresponding diagonal element of the dipolar

coupling tensor $\overleftrightarrow{A}_{\rm dip}$ which possesses the property $\mathrm{tr}(\overleftrightarrow{A}_{\rm dip}) = 0$. $A_i^{\rm con}$ is the contact hyperfine coupling parameter which is usually considered to be isotropic and temperature independent. As we will see, this assumption is frequently not justified, in particular in all the compounds looked at so far which display quadrupolar ordering. K_i^0 is a temperature independent contribution, usually small and positive and thought to arise from the Pauli paramagnetism of the conduction electrons. However, K_i^0 can show both signs and assumes in exceptional cases huge values [30], features not understood at all. So 'normally' the temperature dependence of K_i originates solely from $\chi_i(T)$ and one expects to find that $K_i(T)$ scales with $\chi_i(T)$.

For the considered class of compounds this scaling expectation is more often than not violated, in particular at low temperatures. This feature is also seen in nuclear Knight shifts (see e.g. [31]). Possible reasons for this are:

(i) The conduction electron spin density induced via the RKKY mechanism carries more information on the state of the f-shells than what is contained in the magnetic susceptibility function $\chi_{\rm f}$. This is discussed in section 3 and it is shown that, in general, (except for states with angular momentum $L = 0$) $A^{\rm con}$ can become anisotropic and temperature dependent.

(ii) The magnetic susceptibility of the f-electron atoms next to the μ^+ is different from the bulk susceptibility. This may be relevant in systems which consist of different sublattices of f-electron atoms like in UPd_3 [25]. The contact hyperfine field at the μ^+ may arise mostly from one type of the f-electron atoms and hence one should use in equation (2.1) the susceptibility related to those atoms. However, the relevant sublattice susceptibility is usually not or not very well known.

(iii) A more important deviation of the local $\chi^{\rm loc}$ from the bulk $\chi^{\rm bulk}$ may be induced by the presence of the μ^+. The μ^+ will modify the crystalline electric field (CEF) at the neighbouring f-electron atoms and consequently their CEF splitting, and hence modifies the susceptibility of those atoms. This effect has been clearly demonstrated in μ^+ Knight shift measurements in $PrNi_5$ [32], $PrIn_3$ [33], and $TmNi_2B_2C$ [34] and has been used to prove the importance of CEF effects in UNi_2Al_3 and UPd_2Al_3 [35].

Considering the first possibility (i) the RKKY mechanism leads to exchange integrals which depend on the orientation of the shapes of the charge distributions, characterized by their quadrupole and higher moments. This effect may be strongly enhanced in the presence of the μ^+ at an interstitial site in the neighbourhood of the f-electron atom since the conduction electron distribution around the μ^+ will be highly inhomogenous, due to the formation of a conduction electron screening cloud [37]. This disturbance in the conduction electron distribution introduced by the μ^+ may render quadrupolar effects more visible in the μ^+ Knight shift than in nuclear Knight shifts. We do not consider here the possible modification of the RKKY coupling of two f-electron atoms when the μ^+ is placed between them.

In section 3 the role of the orbital exchange mechanism in determining the contact coupling parameter will be discussed, leading to a qualitative explanation of some of the observed 'anomalous' features of $A^{\rm con}$ in the presented μSR data. In the following we will review and discuss the evidence for quadrupolar effects in the μ^+ Knight shift. The compounds studied are HoB_2C_2, CeB_6, CeAg, $PrCu_2$ and UPd_3.

2.2. HoB_2C_2

This compound was the first one which revealed clearly that the loss of scaling in the K versus χ plot could not have been induced entirely by the μ^+ [38]. The transverse field (TF) measurements at $H_{\rm ext} = 6$ kOe revealed a single component when $\boldsymbol{H}_{\rm ext} \parallel c$-axis and two components with equal weight when $\boldsymbol{H}_{\rm ext} \perp c$-axis [38]. Figures 5(a)–(c) display the

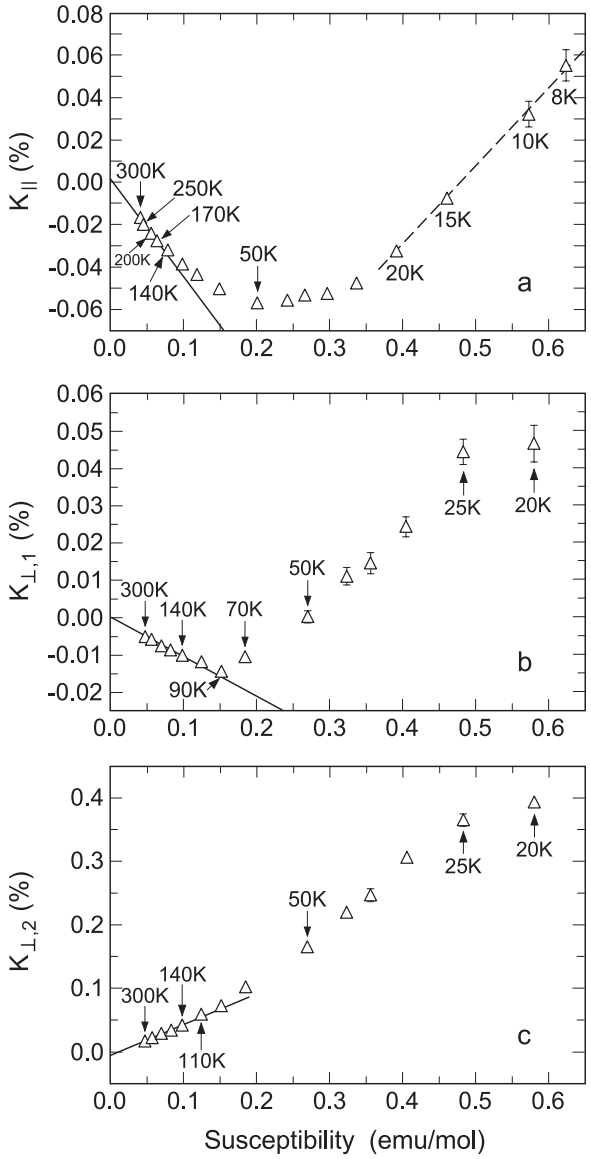

Figure 5. Plot of the μ^+ Knight shift in HoB_2C_2 versus magnetic susceptibility for (a) $\boldsymbol{H}_{\rm ext} \parallel c$-axis (only one component present), (b), (c) for $\boldsymbol{H}_{\rm ext} \perp c$-axis (two components present) (adapted from [38]).

extracted Knight shifts for the three components versus the bulk magnetic susceptibility χ_i. As can be seen, the Knight shift K_i scales with the bulk χ_i at high temperatures. From the high temperature slopes it was possible to determine the μ^+ site in the usual way [29]. It is the 8i site at a distance of 1.7 Å from the nearest Ho ion (see figure 6). More instructive is the fact that $K_\parallel$ and $K_{\perp 1}$ show a zero crossing and a reversed slope $\mathrm{d}K_i/\mathrm{d}\chi_i^{\rm bulk}$ at and below about 14 and 50 K respectively. At the crossing point equation (2.1) becomes

$$\left(A^{\rm dip}_{\parallel,\perp 1} + A^{\rm con}_{\parallel,\perp 1}\right)\chi^{\rm loc}_{\parallel,\perp}(T) + K^0_{\parallel,\perp 1} = 0. \tag{2.2}$$

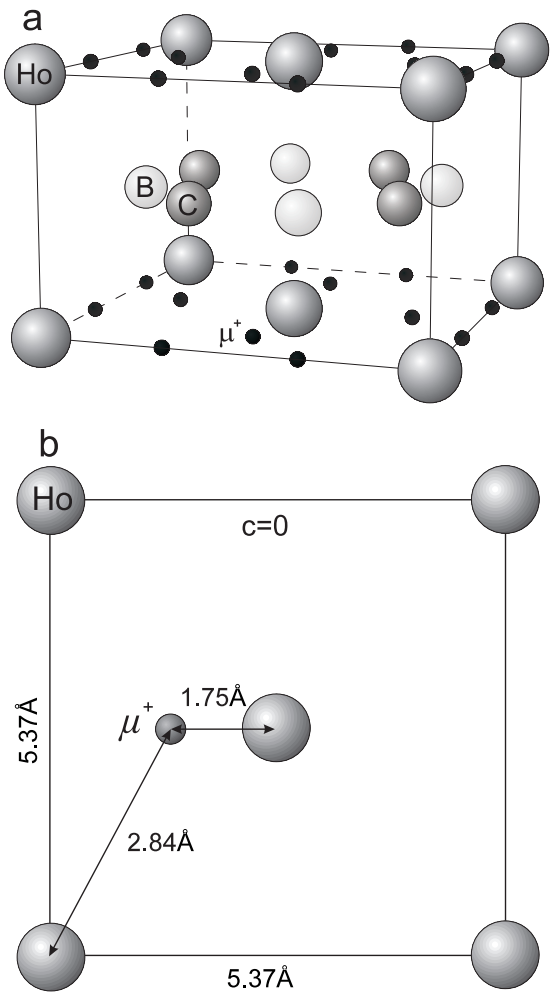

Figure 6. Schematic plot of the crystal structure of tetragonal HoB_2C_2. The μ^+ sites (8i) are also indicated in the upper panel. The lower panel shows the precise location of one of the μ^+ sites (from [38]).

Since, as can be read from figures 5(a), (b), $K^0_{\parallel,\perp 1}$ is rather small ($K^0_{\parallel} = -5.7(8)\times 10^{-3}$, $K^0_{\perp 1} = -3.6(5)\times 10^{-3}$) and $K^0_{\parallel,\perp,i}/\chi^{\rm bulk}_{\parallel,\perp} = 0.005$–$0.007\ {\rm kG}/\mu_{\rm B} \simeq 0$ at the zero crossing points we find

$$A^{\rm dip}_{\parallel,\perp 1} + A^{\rm con}_{\parallel,\perp 1} \simeq 0. \tag{2.3}$$

Since $A^{\rm dip}_{\parallel,\perp 1,2}$ can be extracted from the high temperature slopes ${\rm d}K_{\parallel,\perp 1,2}/{\rm d}\chi_{\parallel,\perp}$ ($A^{\rm dip}_{\parallel} = -2.42\ {\rm kG}/\mu_{\rm B}$, $A^{\rm dip}_{\perp 1} = -0.43\ {\rm kG}/\mu_{\rm B}$, $A^{\rm dip}_{\perp,2} = 2.86\ {\rm kG}/\mu_{\rm B}$), $A^{\rm con}_{\parallel,\perp 1}$ are rather well determined at the crossing points without having to know $\chi^{\rm loc}_{\parallel,\perp}$ or $\chi^{\rm bulk}_{\parallel,\perp}$ (solid circle and star in figure 7). Note that in the measurements the orientation of $\boldsymbol{H}_{\rm ext}$ in the basal plane was not parallel to the a- or b-axis but tilted by $\sim 21^\circ$ from the a-axis [38]. Hence $A^{\rm dip}_{\perp i}$ are not to be identified with $A^{\rm dip}_{\rm aa}$ or $A^{\rm dip}_{\rm bb}$. In the high temperature scaling regime $\chi^{\rm loc}_{\parallel,\perp} = \chi^{\rm bulk}_{\parallel,\perp}$. Assuming that this identity also holds at lower temperature ($\lesssim 100$ K), we can extract $A^{\rm con}_{\parallel,\perp 1,2}(T)$ from $K_{\parallel,\perp 1,2}(T)$ using

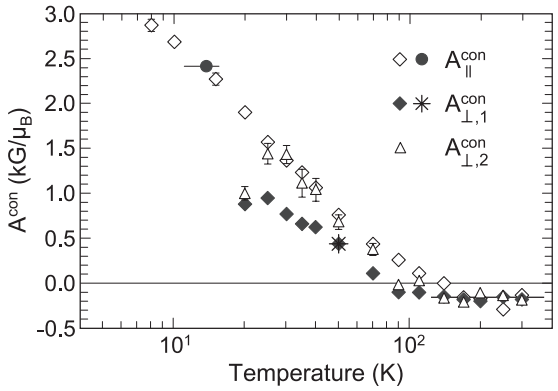

Figure 7. Temperature dependence of the contact coupling parameters, A^{con}, extracted from $K_{\parallel}(T)$ and $K_{\perp i}(T)$ in HoB_2C_2. The star and the filled circle follow directly from the zero crossing of $K_{\parallel}(T)$ and $K_{\perp 1}(T)$ at particular temperatures without having to know the relevant susceptibilities.

equation (2.1). The results are displayed in figure 7. Should $\chi^{loc}(T)$ deviate from $\chi^{bulk}(T)$ at lower temperatures, $A^{con}_{\parallel,\perp}(T)$ would, of course, look different but would be unchanged at the zero-crossing temperature. Hence the overall behaviour of $A^{con}_{\parallel,\perp}(T)$ would in any case not be drastically different from that shown in figure 7.

As figure 7 reveals, the contact coupling constants $A^{con}_{\parallel,\perp 1,2}$ become temperature dependent below ∼150 K, change from negative to positive, and develop a partial anisotropy, particularly in the basal plane. Apparently it matters whether the shortest μ^+–Ho distance is oriented parallel or perpendicular to the applied field. These observations point to a scenario in which the RKKY induced conduction-electron-spin polarization depends on the orientation of the Ho 4f quadrupole moments with respect to screening cloud around the μ^+, i.e. to the first possibility (i). Within this scenario the quadrupole moments are randomly oriented above ∼100 K, resulting in a temperature independent and isotropic A^{con}, followed, below 100 K, by a regime in which the quadrupole moments start to order, e.g. by aligning collinearly with the induced magnetic moments, i.e. a kind of field induced ferro- or antiferro- or more complicated quadrupolar state is established, depending on which arrangement leads to the lowest energy. Unfortunately it was not possible to extend the measurements down to the onset of the spontaneous antiferroquadrupolar state at 4.5 K since it was masked by the magnetic order setting in at 5.9 K [19].

If the suggested scenario is correct, HoB_2C_2 would be the first compound where a field induced quadrupolar order was observed. This would find its counterpart in the field induced magnetic order observed in some compounds in the quadrupolar phase, e.g. in CeB_6. Our model may be checked by careful measurements of the temperature dependence of the lattice constants and other relevant bulk parameters in the presence of $H_{ext} > 0$. Finally, by inspecting figures 5(a)–(c), one might get the impression that $K_{\parallel\perp 1,2}$ scales again with $\chi_{\parallel,\perp}$ at low temperatures, i.e. below 20–50 K. The data are indeed fitted very well by a straight line, but the temperature independent $K^0_{\parallel,\perp 1,2}$ show drastically different and unphysically large negative values. In particular $K^0_{\parallel,\perp 1,2}$ would become strongly temperature dependent in the region between the two scaling regimes. Hence the apparent scaling at low T is to be viewed as accidental. This was not recognized in [38]. However, at high T the μ^+ induced change of the CEF level scheme has a negligible effect on the susceptibility and hence $K \propto \chi \propto 1/T$ and the scaling is not accidental.

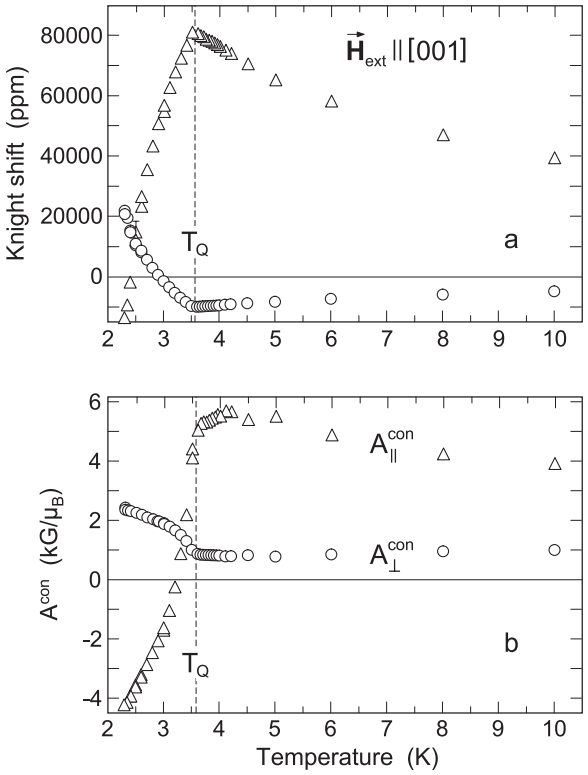

Figure 8. (a) Temperature dependence of the two Knight shifts in CeB_6 associated with the two magnetically inequivalent d sites for $\boldsymbol{H}_{ext} \parallel [001]$, (b) extracted contact coupling parameters, $A^{con}_{\parallel}$, $A^{con}_{\perp}$. The symbols $\parallel$ and $\perp$ indicate whether the applied field (6 kOe) is parallel or perpendicular to the distance vector connecting the μ^+ and the nearest Ce^{3+} neighbours. Note that A^{con} is already anisotropic above T_Q.

2.3. CeB_6

CeB_6 is *the* compound which shows the transition into the antiferroquadrupolar state most pronouncedly reflected in the muon Knight shift as figure 8(a) clearly demonstrates [39]. The shifts above ∼10 K up to 200 K (the highest temperature investigated) scale perfectly with the bulk susceptibility. The TF signal consists of two components with an amplitude ratio of 2:1. This is to be expected since the only two reasonable interstitial sites in this cubic system, the d and c sites (see figure 9), split into two magnetically inequivalent subsets with an abundance ratio likewise of 2:1. If one proceeds in the usual way, assuming that A^{con} is isotropic and temperature independent one finds from the high temperature slopes of K versus χ that $A^{dip}_{zz} = 5.93\,\mathrm{kG}/\mu_B$ and $A^{con} = 1.85\,\mathrm{kG}/\mu_B$. The calculated values of A^{dip}_{zz} for the d and c sites are $3.94\,\mathrm{kG}/\mu_B$ and $-1.14\,\mathrm{kG}/\mu_B$, respectively. Hence the measured value is far from the expected values for the two possible sites. A lattice distortion around the μ^+ as a possible origin of this discrepancy can be excluded since it would imply a giant local lattice *contraction* of ∼14%, while generally a lattice *expansion* of a few per cent is found around μ^+ or protons (hydrogen) in metals. On the other hand, Saitoh *et al* [40] claimed on the basis of polarized neutron diffraction measurements that a sizable fraction of the field induced magnetization or spin polarization is found at distinct positions inside and outside of the B_6 octahedron. This

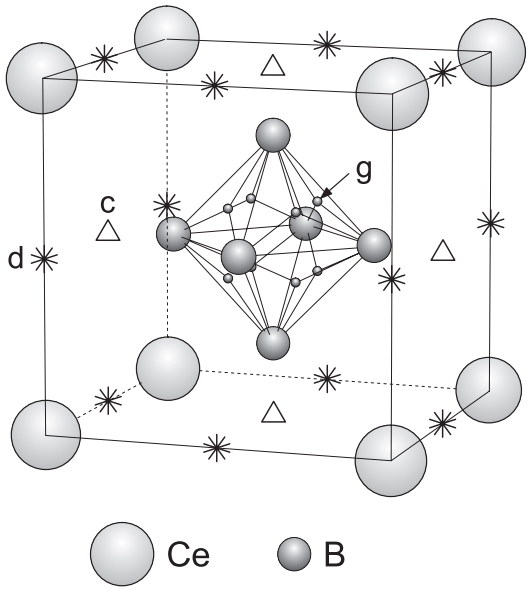

Figure 9. Crystal structure of cubic CeB_6. The μ^+ are located at the interstitial d sites.

additional source for fields at the μ^+ site, suggested to be the d site, allowed an explanation of the discrepancy with very reasonable implications for the induced spin polarization inside and around the B_6 complex [39]. However, in the meantime it became clear that the original claim of Saitoh *et al* was probably incorrect, and no magnetization density is associated with the B_6 complex [41]. Hence the discrepancy between the calculated and extracted A^{con} had to be attributed to a different source. The solution is to drop the conventional assumption that A^{con} is isotropic.

Assigning the μ^+ to the d site, which is more spacious than the c site (at the c site the distance to the nearest B neighbour is only 0.83 Å, which appears too small to allow the μ^+ to reside there), and taking the calculated A_{zz}^{dip} as the true value, A^{con} can be extracted above 10 K from the slopes $\mathrm{d}K/\mathrm{d}\chi$. For example, if H_{ext} is oriented parallel to the [001]-axis, defined to be the z-axis, the d sites with $z = \frac{1}{2}$ possess the slope

$$\frac{\mathrm{d}K_{\parallel}}{\mathrm{d}\chi} = \left(A_{\parallel}^{\mathrm{con}} + A_{zz}^{\mathrm{dip}}\right) = 7.89\ \mathrm{kG}/\mu_{\mathrm{B}}$$

and the d site with $z = 0$ or 1 (there are twice as many as with $z = \frac{1}{2}$)

$$\frac{\mathrm{d}K_{\perp}}{\mathrm{d}\chi} = \left(A_{\perp}^{\mathrm{con}} - \frac{1}{2}A_{zz}^{\mathrm{dip}}\right) = -0.97\ \mathrm{kG}/\mu_{\mathrm{B}}.$$

The parallel and perpendicular symbols refer to the relative orientation of the induced nearest neighbour (nn) Ce 4f moment and the distance vector μ^+–nn Ce. We find $A_{\parallel}^{\mathrm{con}} = 3.94\ \mathrm{kG}/\mu_{\mathrm{B}}$ and $A_{\perp}^{\mathrm{con}} = 1.01\ \mathrm{kG}/\mu_{\mathrm{B}}$.

The angular dependence of the Knight shift of the two components has been measured in the case that $\boldsymbol{H}_{\mathrm{ext}}$ is rotated in a $(1\bar{1}0)$-plane by turning the crystal around the $[1\bar{1}0]$-axis; see figure 10. Theoretically one expects that [39]

$$K_{z=\frac{1}{2}}(\theta) = K_1^0 + \left(A_{z=\frac{1}{2}}^{\mathrm{con}}(\theta) + A_{zz}^{\mathrm{dip}}P_2^0(\cos\theta)\right)\chi, \tag{2.4}$$

$$K_{z=0,1}(\theta) = K_2^0 + \left(A_{z=0,1}^{\mathrm{con}}(\theta) - \tfrac{1}{2}A_{zz}^{\mathrm{dip}}P_2(\cos\theta)\right)\chi, \tag{2.5}$$

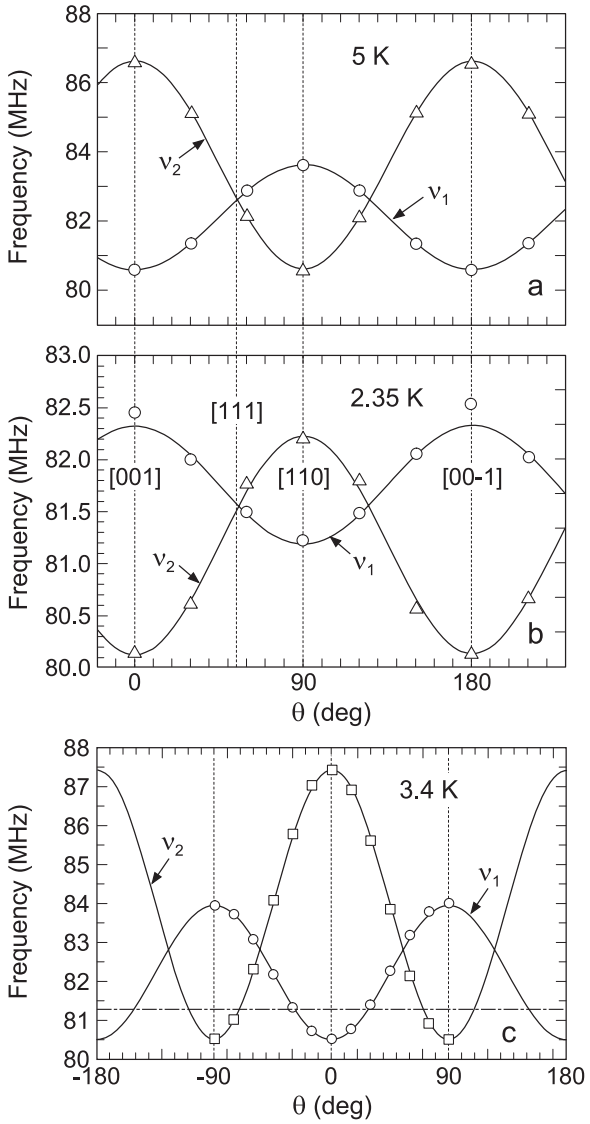

Figure 10. Orientation dependence of the two precession frequencies ν_1, ν_2 in CeB_6 at (a) 5 K, (b) 2.35 K, (c) 3.4 K. The applied field $\boldsymbol{H}_{\rm ext}$ is rotated in a $(1\bar{1}0)$-plane and θ is the angle between the [001]-axis and $\boldsymbol{H}_{\rm ext}$. The solid lines represent fits of the form of equation (2.6) yielding generally $A_2 = -1/2A_1$, but note that below 2.5 K A_1 and A_2 have changed their signs. The temperature at which this happens is field dependent (not shown).

where $A_i^{\rm con}(\theta)$ are not known *a priori* and θ is the angle between $\boldsymbol{H}_{\rm ext}$ and the [001]-axis. Experimentally one finds

$$K_i(\theta) = K_i^0 + A_i P_2(\cos\theta)\chi \tag{2.6}$$

with $A_2 = -(1/2)A_1$, implying that $A_i^{\rm con}(\theta) = A_i^{\rm con} P_2(\cos\theta)$ with also $A_2^{\rm con} = -(1/2)A_1^{\rm con}$. This is observed above $T_{\rm Q}$ as well as below $T_{\rm Q}$ at 3.4 K and at 2.35 K (just above $T_{\rm N}$); see figure 10. This is a puzzling outcome since it suggests that the contact hyperfine field possesses a dipolar character, which is not expected. However, considering that $A^{\rm con}$ refers to the spin

polarization of the conduction electrons at the μ^+ site induced via the RKKY mechanism by the induced moments on the Ce sites, and that the RKKY coupling depends on the orientation of the 4f quadrupole moments (see section 3), and, further, that in the Γ_8 quartet state the quadrupole moment can easily follow the magnetic dipole moment, suggests the use of the ansatz

$$A^{\mathrm{con}}(\theta) = \sum_j A^*_{\perp,j} \sin^2 \vartheta_j + A^*_{\parallel,j} \cos^2 \vartheta_j, \tag{2.7}$$

where the sum extends over the nearest Ce neighbour sites (only two in CeB_6) and ϑ_j is the angle between the induced moment at site j and the distance vector connecting the site j with the μ^+ site (a d site in the present case). $A^*_{\parallel,\perp}$ are to be viewed as coupling constants parallel and perpendicular to the distance vector connecting the μ^+ and a nearest Ce^{3+} ion. Note that the direction of the contact hyperfine field is given by the direction of the generating 4f-moment and hence A^{con} cannot be cast into tensorial form. But see also the discussion in section 3.

For the μ^+ sites with $z = \frac{1}{2}$, ϑ_j is just given by the angle between $\boldsymbol{H}_{\mathrm{ext}}$ and the [001]-axis, i.e. $\vartheta = \theta$ and hence equation (2.7) becomes

$$A^{\mathrm{con}}_{z=\frac{1}{2}}(\theta) = \tfrac{2}{3}\left(A^*_\parallel + 2A^*_\perp + 2(A^*_\parallel - A^*_\perp) P_2(\cos\theta)\right). \tag{2.8}$$

For the sites with $z = 0, 1$

$$\cos\vartheta = \frac{1}{\sqrt{2}} \sin\theta, \tag{2.9}$$

and hence

$$A^{\mathrm{con}}_{z=0,1}(\theta) = \tfrac{2}{3}\left(A^*_\parallel + 2A^*_\perp - (A^*_\parallel - A^*_\perp) P_2(\cos\theta)\right). \tag{2.10}$$

Thus we find that the prefactors of $P_2(\cos\theta)$ also display the ratio $-1/2$. The reason for this outcome can be traced back to the circumstance that $\boldsymbol{H}_{\mathrm{ext}}$ was turned in the $(1\bar{1}0)$-plane which for the sites with $z = 0, 1$ leads to the factor $1/\sqrt{2}$ in equation (2.9). Further, $A^{\mathrm{con}}_\parallel = 2A^*_\parallel$ and $A^{\mathrm{con}}_\perp = 2A^*_\perp$. The correct reproduction of the experimental angular dependence of the Knight shifts on the basis of equation (2.7) above and below T_{Q} seems to confirm the assumption that the quadrupole moment follows the magnetic dipole moment in phase I as well as in phase II. The latter is also predicted theoretically [10].

So far we have mainly only considered the Knight shift results above 10 K in the scaling regime. As figure 8(a) shows, a dramatic change happens when the temperature drops below T_{Q} and both $K_\parallel$ and $K_\perp$ pass through zero at ∼2.3 and 3.9 K, respectively. However, the orientational dependence, as emphasized above, is still given by equations (2.4), (2.5) and (2.7). Assuming that the local susceptibility continues to be equal to the bulk susceptibility we can extract $A^{\mathrm{con}}_\parallel$ and $A^{\mathrm{con}}_\perp$ as in the case of HoB_2C_2; see figure 8(b). Since, like in HoB_2C_2, the temperature independent $K^0_{\parallel,\perp}$ are relatively small ($K^0_\parallel \simeq -350$ ppm, $K^0_\perp \simeq 114$ ppm) the zero crossing of $K^0_{\parallel,\perp}$ allows one again to extract $A^{\mathrm{con}}_{\parallel,\perp}$ at these temperatures without having to know the relevant magnetic susceptibility to any precision. The thus determined $A^{\mathrm{con}}_{\parallel,\perp}$ fall nicely on top of the data in figure 8(b). $A^{\mathrm{con}}_{\parallel,\perp}$ shows a strong temperature dependence and $A^{\mathrm{con}}_\parallel$ even changes its sign below about 3.2 K. The transition temperature T_{Q} is clearly manifest in the data and $A^{\mathrm{con}}_\parallel$ seems to reveal a second anomaly at ∼4.1 K of unknown origin. Evidently, below T_{Q}, the antiferroquadrupolar order must lead to drastically changed contact coupling constants, pointing to different average non-spherical charge distributions of the 4f electrons, alternating from Ce site to Ce site, and to a lifting of the degeneracy of the quartet ground state. The temperature dependence of $A^{\mathrm{con}}_{\parallel,\perp}$ below but close to T_{Q} follows the relation $(1 - T/T_{\mathrm{Q}})^\beta$ with $\beta \simeq 1/3$, which is essentially the same as found for the antiferroquadrupolar order

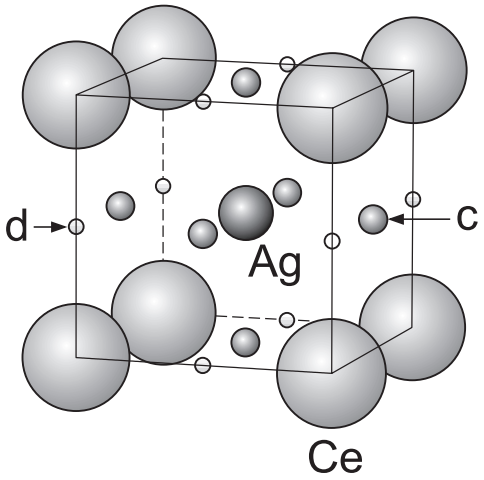

Figure 11. Crystal structure of cubic CeAg. The μ^+ is most likely located at the c site in a (001)-plane.

parameter in [11]. Hence it appears that $A^{\rm con}_{\parallel,\perp}$ mirrors directly the temperature dependence of the order parameter [42].

In view of the suggestion that field induced magnetic octupole moments play an important role in phase II one might wonder whether the fields arising from the octupole moments could not explain the drastic temperature dependence of the μ^+ Knight shift below $T_{\rm Q}$. If so, however, the octupolar fields must become of the same order of magnitude as the dipolar and contact fields, which is considered to be most unlikely (see also section 6).

2.4. CeAg

The crystal structure of cubic CeAg is very similar to CeB_6. The Ag atom replaces the B_6 complex and the available interstitial sites are again the c and d sites (see figure 11). According to [43] the muon is most likely located at the c site, unlike the situation in CeB_6.

In addition a second site is found which may be a vacancy in the Ag sublattice and which is occupied by about 13% of the implanted μ^+. This fraction will not concern us further here.

We begin with a discussion of the angular dependence of the Knight shifts associated with the c site when $H_{\rm ext}$ is rotated in the (001)-plane [43]. In general we find three components in the TF signal with equal amplitudes, as is to be expected when $\boldsymbol{H}_{\rm ext}$ is not parallel to the [010]-axis or the [100]-axis. This is in contrast to the case that $\boldsymbol{H}_{\rm ext}$ is rotated, e.g. in the $(1\bar{1}0)$-plane (see the previous discussion in the case of CeB_6). The c site is now split into three magnetically inequivalent subsites, represented by the sites $(\frac{1}{2}\frac{1}{2}0)$, $(0\frac{1}{2}\frac{1}{2})$ and $(\frac{1}{2}0\frac{1}{2})$. For these sites we write [43]

$$K(\varphi)_{(0\frac{1}{2}\frac{1}{2})} = \left[A^{\rm con}_{(0\frac{1}{2}\frac{1}{2})}(\varphi) + \tfrac{1}{2}\left(A^{\rm dip}_{xx} + A^{\rm dip}_{yy} + \left(A^{\rm dip}_{xx} - A^{\rm dip}_{yy}\right)\cos 2\varphi\right)\right]\chi, \quad (2.11)$$

$$K(\varphi)_{(\frac{1}{2}0\frac{1}{2})} = \left[A^{\rm con}_{(\frac{1}{2}0\frac{1}{2})}(\varphi) + \tfrac{1}{2}\left(A^{\rm dip}_{xx} + A^{\rm dip}_{yy} + \left(A^{\rm dip}_{yy} - A^{\rm dip}_{xx}\right)\cos 2\varphi\right)\right]\chi, \quad (2.12)$$

$$K(\varphi)_{(\frac{1}{2}\frac{1}{2}0)} = \left[A^{\rm con}_{(\frac{1}{2}\frac{1}{2}0)}(\varphi) + A^{\rm dip}_{yy}\right]\chi, \quad (2.13)$$

where φ is the angle between $H_{\rm ext}$ and the [100]-axis. The $A^{\rm dip}_{ii}$ for the c site are calculated to be $A^{\rm dip}_{xx} = -1.528$ kG/$\mu_{\rm B}$, $A^{\rm dip}_{yy} = +0.764$ kG/$\mu_{\rm B}$. Hence we should find two shifts,

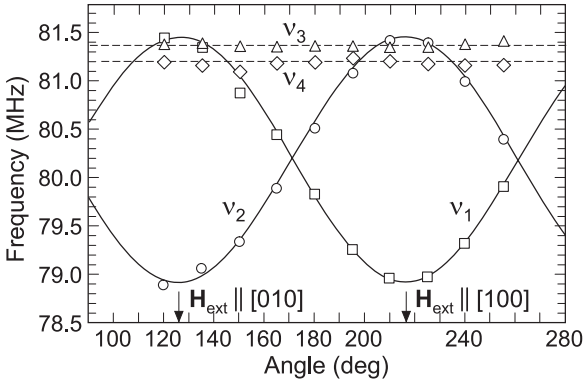

Figure 12. Orientation dependence of the precession frequencies ν_i ($i = 1, 2, 3$) in CeAg at 25 K when $\boldsymbol{H}_{\rm ext}$ (6 kOe) is rotated in an (001)-plane. Note the splitting of the ν_i ($i = 1, 2, 3$) for $\boldsymbol{H}_{\rm ext} \parallel$ [100] or $\parallel$ [010]. The fourth frequency ν_4 arises probably from μ^+ located at an Ag vacancy (from [43]).

which are dependent on φ and shifted by 90° with respect to each other, and one shift, which is orientation independent. Further, for $\varphi = 0$, $K(0)_{(\frac{1}{2}0\frac{1}{2})} = K(0)_{(\frac{1}{2}\frac{1}{2}0)}$ and for $\varphi = 90°$, $K(90°)_{(0\frac{1}{2}\frac{1}{2})} = K(0)_{(\frac{1}{2}\frac{1}{2}0)}$ as long as $A^{\rm con}$ is isotropic. These expectations are well followed by the measurements at 25 K (see figure 12) except that the degeneracies for $\boldsymbol{H}_{\rm ext} \parallel$ [100]-axis and $\boldsymbol{H}_{\rm ext} \parallel$ [010]-axis are not observed. A small significant splitting is clearly present as the overall φ-dependence reveals. A misalignment can be excluded because $K(\varphi)_{(\frac{1}{2}\frac{1}{2}0)}$ should become orientation dependent, which is not observed. Since the susceptibility is isotropic and the crystal structure at 25 K still cubic, it follows that the splitting has to be attributed to the contact coupling parameter $A^{\rm con}$ which must become anisotropic. We find again agreement with the data if we express $A^{\rm con}(\varphi)$ by

$$A^{\rm con}(\varphi) = \sum_{i=1}^{4} \left[\sin^2\theta_i \left(\cos^2\Phi_i A^*_{x'x'} + \sin^2\Phi_i A^*_{y'y'}\right) + \cos^2\theta_i A^*_{z'z'}\right], \qquad (2.14)$$

which, if all the A^*_{ii} were positive, describes a non-axially symmetric ellipsoid. The x', y', z' refer to a coordinate system where the z'-axis is parallel to the [001]-axis and the x'-axis is parallel to $\boldsymbol{H}_{\rm ext}$ or the induced $\boldsymbol{\mu} = \chi \boldsymbol{H}_{\rm ext}$. The angles θ_i and Φ_i are the direction angles of the distance vector connecting the μ^+ and one of the nearest Ce neighbours. The sum runs over the four nearest Ce neighbours around the c site. This equation is analogous to equation (2.7), except that it allows for the possibility that also perpendicular to $\boldsymbol{\mu}$ we have anisotropic coupling parameters defined with respect to the [001]-axis. In CeB_6 we had assumed $A^*_{x'x'} = A^*_{y'y'} = A^*_{\perp}$. Equation (2.14) allows us to rewrite the $A^{\rm con}(\varphi)$ in equations (2.11)–(2.13) as follows [43]:

$$A^{\rm con}_{(0\frac{1}{2}\frac{1}{2})}(\varphi) = 2A^*_{z'z'} + A^*_{y'y'} + A^*_{x'x'} + \left(A^*_{y'y'} - A^*_{x'x'}\right)\cos 2\varphi \qquad (2.15)$$

$$A^{\rm con}_{(\frac{1}{2}0\frac{1}{2})}(\varphi) = 2A^*_{z'z'} + A^*_{y'y'} + A^*_{x'x'} + \left(A^*_{x'x'} - A^*_{y'y'}\right)\cos 2\varphi \qquad (2.16)$$

$$A^{\rm con}_{(\frac{1}{2}\frac{1}{2}0)}(\varphi) = 2\left(A^*_{x'x'} + A^*_{y'y'}\right). \qquad (2.17)$$

Equations (2.15)–(2.17) exhibit the same angular dependence as the dipolar contribution in equations (2.11)–(2.13), in particular the absence of any φ-dependence at the $(\frac{1}{2}\frac{1}{2}0)$ site, but the degeneracy at $\varphi = 0°$ and 90° is now lifted provided that $A^*_{x'x'} \neq A^*_{y'y'}$. So the qualitative behaviour of the observed Knight shifts allows us already to conclude that the contact coupling

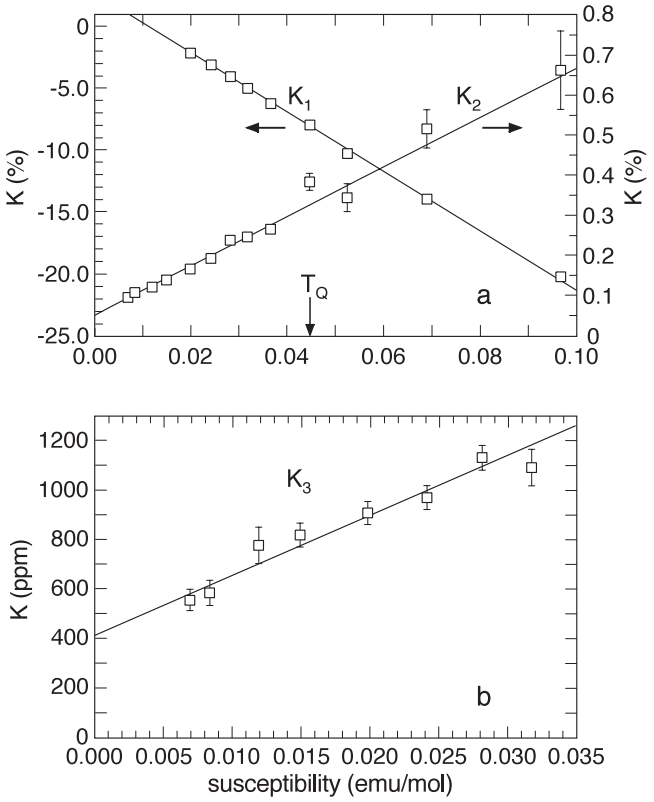

Figure 13. Clogston–Jaccarino plots of Knight shift versus susceptibility in CeAg: (a) K_1, K_2; (b) K_3 for $\boldsymbol{H}_{\rm ext} \parallel [100]$ (from [43]).

parameters are anisotropic, and this conclusion is not dependent on the assumed μ^+ site. The anisotropy is not restricted to the temperature regime below $T_{\rm Q}$ but occurs as well above $T_{\rm Q}$ as in CeB_6, and, below $\sim$100 K, in HoB_2C_2 and $PrCu_2$ (see section 2.5). Again it seems that some field induced quadrupolar state is formed above $T_{\rm Q}$. The temperature dependence of $K_{(0\frac{1}{2}\frac{1}{2})}$, $K_{(\frac{1}{2}0\frac{1}{2})}$ and $K_{(\frac{1}{2}\frac{1}{2}0)}$, measured for $\varphi = 0$, reveals that the Knight shifts scale with the susceptibility from approximately 10 K up to 90 K. Above 90 K, μ^+ diffusion was observed to set in and all three components collapsed into a single component around 150 K. In contrast to CeB_6, the transition into the ferroquadrupolar state was not reflected in the Knight shift data. The transition temperature $T_{\rm Q} \simeq 15$ K is well situated in the scaling regime of $K_{(0\frac{1}{2}\frac{1}{2})}$ and $K_{(\frac{1}{2}0\frac{1}{2})}$ (see figure 13), and hence the $A^{\rm con}$ do not change when passing from the paramagnetic phase into the ferroquadrupolar state. This could indicate that the field induced quadrupolar order above $T_{\rm Q}$ and the spontaneous ferroquadrupolar below $T_{\rm Q}$ are identical. Below $T_{\rm Q}$ the only effect of $\boldsymbol{H}_{\rm ext}$ is to induce a single domain ferroquadrupolar state. In contrast, in CeB_6, in view of the strong anomaly of $A^{\rm con}$ at $T_{\rm Q}$, the field induced quadrupolar state must be quite different from the spontaneous antiferroquadrupolar order below $T_{\rm Q}$.

Analyzing the scaling regime with the assumption that the contact coupling parameter is isotropic, one arrives at $A^{\rm dip}_{xx} = 4.23$ kG/$\mu_{\rm B} = -\frac{1}{2}A^{\rm dip}_{yy}$ [43], to be compared with the calculated values for the c and d sites of 0.764 kG/$\mu_{\rm B}$ and -2.644 kG/$\mu_{\rm B}$, respectively. The experimental value is far away from the calculated values (as in CeB_6; see the discussion in section 2.3), but least far from the c site value. Adopting the c site as the most likely site and

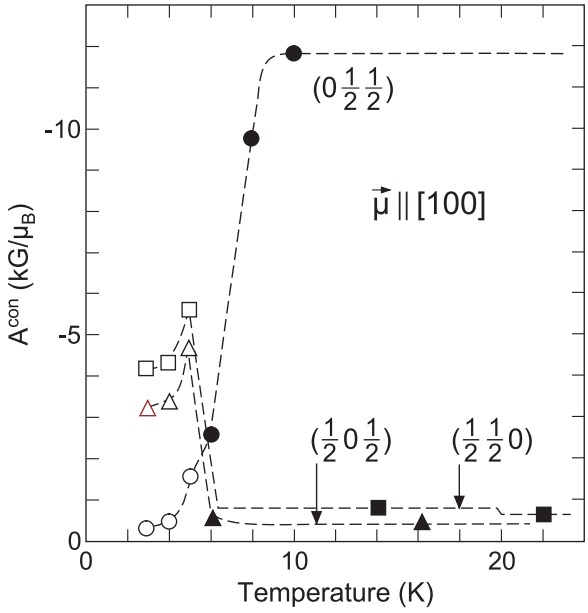

Figure 14. The extracted temperature dependence of $A^{\rm con}$ for $\boldsymbol{H}_{\rm ext} \parallel [100]$ and the different c sites in CeAg. The filled points for $T > T_{\rm c}$ were derived from the K_i, and the open points for $T < T_{\rm c}$ from the spontaneous fields B_i (from [43]).

assuming that $A_{xx}^{\rm dip} = 0.764\ {\rm kG}/\mu_{\rm B}$ is the true value and, further, that $\chi_{\rm loc} = \chi_{\rm bulk}$, one can determine the $A^{\rm con}$ as in the previous cases. The result is displayed in figure 14. The values below $T_{\rm C} = 5.5$ K are derived from the measured spontaneous fields in the ferromagnetic state. These results suggest that the ferroquadrupolar state undergoes some structural change at the Curie temperature $T_{\rm C}$. This possibility must be checked by careful measurement of the tetragonal lattice parameters across $T_{\rm C}$.

A final comment on the implications of the ansatz equation (2.13) is in order. This expression does not only imply that one of the principal axes of the quadrupole moment follows the induced magnetic moment $\boldsymbol{\mu} = \chi \cdot \boldsymbol{H}_{\rm ext}$ but also that a second principal axis is fixed with respect to the crystal axes. In the present case, it is the principal axis along [001] perpendicular to the plane which contains $\boldsymbol{H}_{\rm ext}$.

2.5. $PrCu_2$

The μ^+ Knight shift in $PrCu_2$ appears to be affected by both a μ^+ induced modification of the local susceptibility (i.e. the susceptibility of the Pr ions next to the μ^+) and by quadrupolar effects. Figure 15 displays the measured Knight shift K versus the bulk susceptibility $\chi_{\rm bulk}$ for $\boldsymbol{H}_{\rm ext}$ aligned along the three principle axes of the orthorhombic crystal structure [44]. Note that for $\boldsymbol{H}_{\rm ext} \parallel (a, c)$-plane the TF signal splits below 65 K into two components with equal amplitudes. Here we discuss the average Knight shift of the two components. The splitting is due to the antiferromagnetic order below ∼65 K (see section 4.1). No scaling of K with the susceptibility is found, not even at high temperatures ($T \gtrsim 120$ K), as a closer inspection reveals. On the other hand, in this regime $K(T)$ is very well fitted by the Curie–Weiss relation

$$K_i(T) = \frac{A_i C}{T - T_{{\rm CW},i}} + K_{0,i}, \tag{2.18}$$

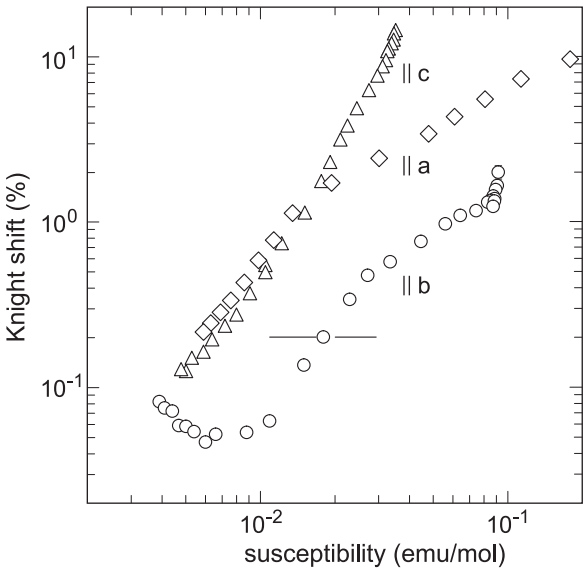

Figure 15. Clogston–Jaccarino plot of Knight shift in $PrCu_2$ for H_{ext} oriented along the a, b and c axes. K_b is shifted up by 0.2% to allow its display on a log scale. The horizontal line corresponds to $K_b = 0$ (from [44]).

Table 1. Collection of fit parameters (equation (2.18)).

	$\boldsymbol{H}_{ext} \parallel \mathbf{a}$	$\boldsymbol{H}_{ext} \parallel \mathbf{c}$	$\boldsymbol{H}_{ext} \parallel \mathbf{b}$
A_i (kG/μ_B)	2.318(3)	0.433(3)	−1.122 fixed[a]
K^0_{ii} (ppm)	−836(24)	188(32)	−515(20)
T_{CW} (K)	96.4(5)	71.8(1.3)	−138(8)
$T_{C,bulk}$ (K)	22.7	−32.7	−102(1)

[a] See text.

where T_{CW} is a Curie–Weiss temperature, $C = NJ(J+1)g_J^2\mu_B^2/3K_b$ the Curie constant, $A_i = A_i^{con} + A_i^{dip}$ $(i = a, b, c)$ the total magnetic coupling constant, and $K_{0,i}$ a temperature independent term. The fit yields T_{CW} which are significantly different from those of the bulk susceptibility, listed in table 1 [44]. Assuming that C is given by the Hund's rule value (=1.6 K emu mol^{-1} for Pr^{3+}) and is not modified by the presence of the μ^+, A_i can be determined. The Curie–Weiss curves for the bulk and the local susceptibility are displayed in figures 16(a)–(c) and the relevant temperature ranges are indicated.

Assuming that A^{con} is isotropic and temperature independent, the dipolar coupling tensor can be determined which leads to the assignment of the μ^+ to the 4e site at the position $(\frac{1}{2}\frac{1}{4}0.613)$, approximately at the centre of the triangle formed by Pr ions (see figure 17). The same site was found in the isostructural compounds $GdCu_2$ [45] and $CeCu_2$ [46]. Vice versa from this agreement we conclude that the assumptions on A^{con} and C were correct. So at high temperatures (i.e. $T \gtrsim 100$ K) we have the same situation concerning the contact coupling parameter as in HoB_2C_2, and quadrupolar effects seem to be absent. The deviation of the local susceptibility from the bulk susceptibility is in this case understood to be a muon induced feature as mentioned earlier in this section. For the orientation $\boldsymbol{H}_{ext} \parallel b$-axis, however, the local χ^{loc} seems to be not much different from χ^{bulk} (figure 16(b)). For $\boldsymbol{H}_{ext} \parallel b$-axis, $K_b(T)$ displays a zero crossing at 40 K (see the inset in figure 16(b))

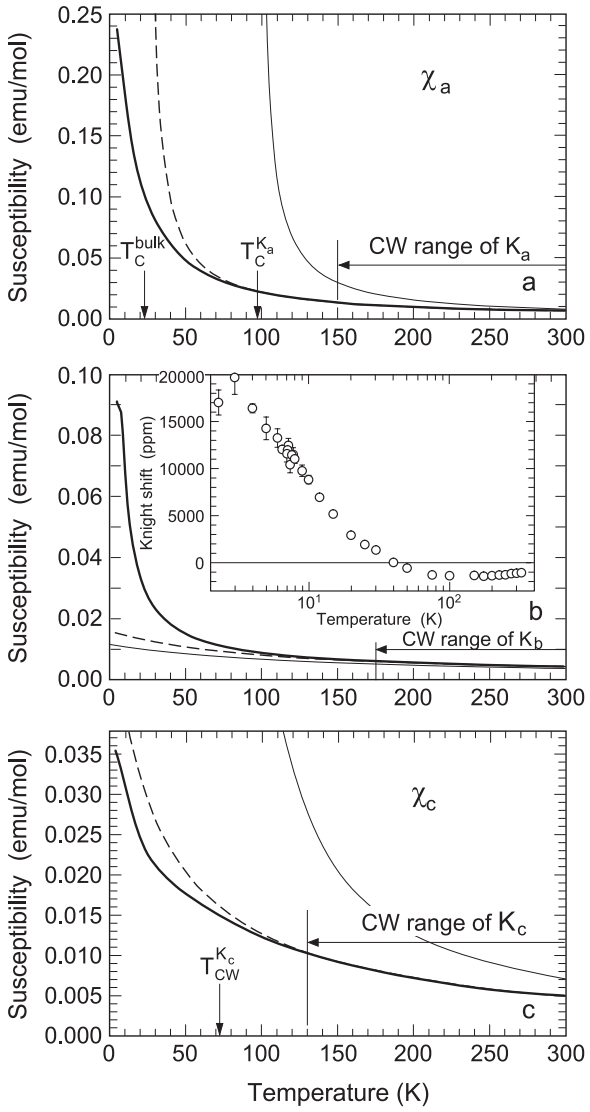

Figure 16. Plot of bulk and local magnetic susceptibility in $PrCu_2$ versus temperature for (a) $\boldsymbol{H}_{\rm ext} \parallel a$-axis, (b) $\boldsymbol{H}_{\rm ext} \parallel b$-axis, (c) $\boldsymbol{H}_{\rm ext} \parallel c$-axis. The fat curves represent the bulk susceptibilities $\chi_i^{\rm bulk}$ (taken from [8]), the dashed curves the Curie–Weiss fits to the high temperature $\chi_i^{\rm bulk}$, and the thin curves the Curie–Weiss fits to high temperature Knight shifts K_i $(i = a, b, c)$, using equation (2.18) with $C = 1.6$ emu mol^{-1}. The range of validity of the Curie–Weiss fit of the K_i is also indicated. The inset in (b) shows the temperature dependence of K_b, revealing the change of its sign at ∼40 K.

which implies, as discussed before, that $A_b^{\rm con}$ must also have become temperature dependent below 120 K so that at 40 K equation (2.2) is fulfilled, i.e. $A_b^{\rm con} = K_b^0/\chi_b - A_{bb}^{\rm dip}$. Since $|K_b^0/\chi_b^{\rm bulk}(40\ {\rm K})| \simeq 0.127\ {\rm kG}/\mu_{\rm B} < |A_{bb}^{\rm dip}| = 1.83\ {\rm kG}/\mu_{\rm B}$ [44], $A_b^{\rm con}(40\ {\rm K}) \simeq -A_{bb}^{\rm dip}$ within 14% even if the local $\chi_b^{\rm loc}$ should be smaller by a factor of 2 than $\chi_b^{\rm bulk}$. But since $\chi_b^{\rm bulk}$ and $\chi_b^{\rm loc}$ are not much different above 150 K we assume that $\chi_b^{\rm loc} \simeq \chi_b^{\rm bulk}$ also below 150 K. With this

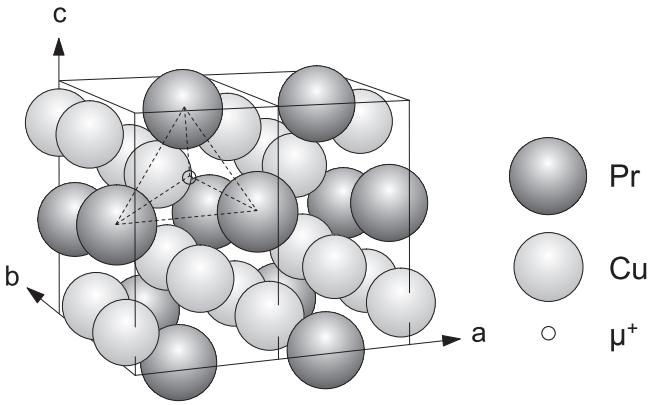

Figure 17. Crystal structure of $PrCu_2$. The μ^+ location at a 4e site is indicated.

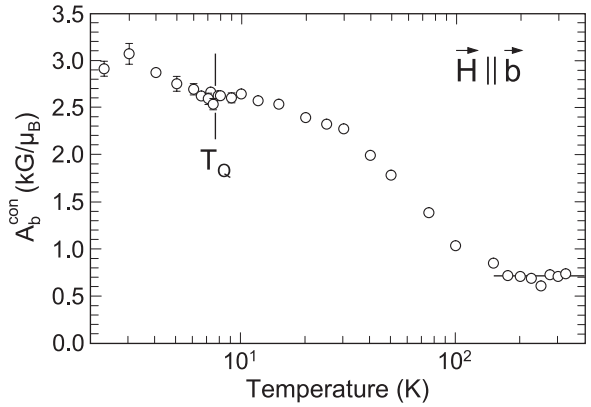

Figure 18. Estimated temperature dependence of $A_b^{\rm con}$ in $PrCu_2$. Note the slight break at $T_{\rm Q}$.

assumption and the known $A_{bb}^{\rm dip}$ we can extract $A_b^{\rm con}(T)$ from $K_b(T)$ as in the previous cases, and $A_b^{\rm con}$ (40 K) is fixed rather well to $-A_{bb}^{\rm dip}$. The results are displayed in figure 18. Because for the two other orientations $\chi_{a,c}^{\rm loc}$ are rather different from $\chi_{a,c}^{\rm bulk}$ already at high temperatures and $K_a(T)$ and $K_c(T)$ do not show a zero crossing, $A_{a,c}^{\rm con}(T)$ cannot meaningfully be extracted from $K_a(T)$ and $K_c(T)$, but it is reasonable to expect that $A_{a,c}^{\rm con}$ become temperature dependent as well. In addition, below 120 K $A_a^{\rm con} \neq A_b^{\rm con} \neq A_c^{\rm con}$, i.e. $A^{\rm con}$ becomes anisotropic. We interpret this again as reflecting a transition from a paraquadrupolar state for $T \gtrsim 120$ K to a partially ordered state below 65 K (i.e. the quadrupolar degrees of freedom are frozen out to a certain extend), which, since it is also observed in zero field measurements (see section 4), appears not to be field induced but may be viewed as a precursor to the ferroquadrupolar order below $T_{\rm Q} \simeq 7.5$ K. Note that $A_b^{\rm con}(T)$ exhibits a change in temperature dependence at $T_{\rm Q}$ (figure 18), although not as strong as in CeB_6. The implications have yet to be worked out.

2.6. UPd_3

UPd_3 played an important role in the development of our understanding that quadrupolar effects are not invisible to μSR [36]. On the other hand the double hexagonal structure of UPd_3 rendered the quantitative analysis of muon Knight shift data impossible due to the fact that

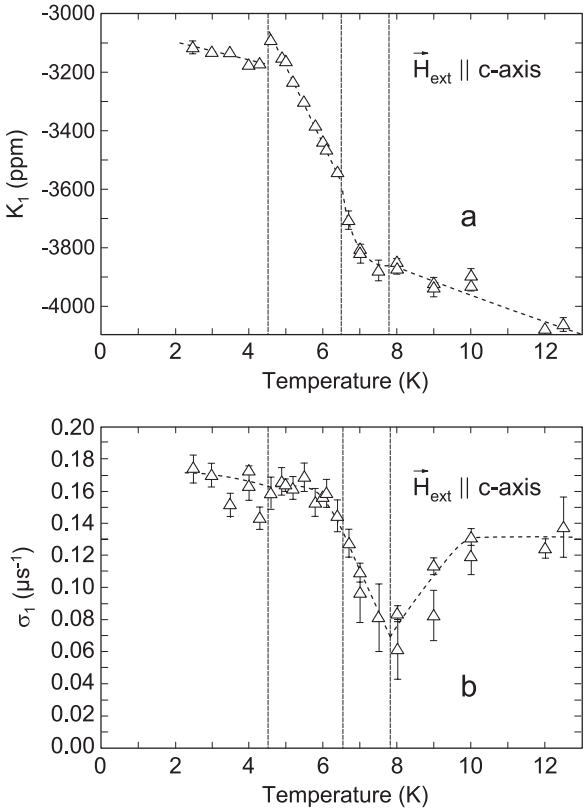

Figure 19. Temperature dependence of (a) K_1 and (b) σ_1 for $\boldsymbol{H}_{\rm ext} \parallel c$-axis in UPd_3. The three transition temperatures are indicated by the dashed vertical lines (from [36]).

the U atoms form two inequivalent sublattices with hexagonal and quasi-cubic symmetry and different magnetic responses, and that no detailed information on the sublattice susceptibilities is available. The TF signal, recorded at $H_{\rm ext} = 6$ kOe, consist of two components with an amplitude ratio of 2:1. The orientation dependence of the two extracted Knight shifts K_1 and K_2 imply that the μ^+ occupy interstitial sites with axial symmetry. The overall temperature dependence of the K_i for $\boldsymbol{H}_{\rm ext} \parallel \boldsymbol{c}$-axis and $\boldsymbol{H}_{\rm ext} \perp \boldsymbol{c}$-axis displayed a complex behaviour with $K_1^{\parallel}$ and $K_1^{\perp}$ crossing zero at different temperatures. But since the Knight shift is induced by U atoms in different sublattices with different magnetic susceptibilities, the zero crossing may just reflect some trivial cancellation features.

Nevertheless, the three transition temperatures T_0, T_1 and T_2 become clearly manifest in the Knight shifts, and in particular also in the Gaussian relaxation rates σ of the TF signals. The anomalies at T_0, T_1 and T_2 are strongest in the dominating component, and we will limit the discussion to this component. Figures 19 and 20 display the temperature dependence of K_1 and σ_1 for $\boldsymbol{H}_{\rm ext} \parallel \boldsymbol{c}$ and $\boldsymbol{H}_{\rm ext} \perp \boldsymbol{c}$. The transition temperatures show up as steps and changes of slopes. It is found that σ_1 as well as σ_2 (not shown) increase proportional to $\boldsymbol{H}_{\rm ext}$, but only below 10 K, i.e. the line broadening appears to be associated with the transition into the quadrupolar ordered regime and not with extrinsic effects, related, for example, to the quality of the single crystal specimen. Above 10 K, σ_1 and σ_2 are close to the Gaussian relaxation rate in zero field [36].

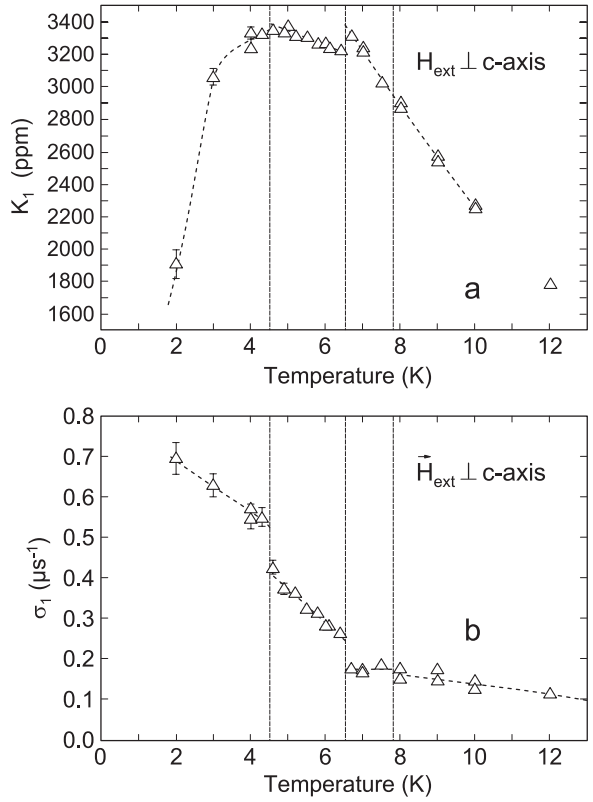

Figure 20. Temperature dependence of (a) K_1 and (b) σ_1 for $\boldsymbol{H}_{\rm ext} \perp c$-axis in UPd_3 (from [36]).

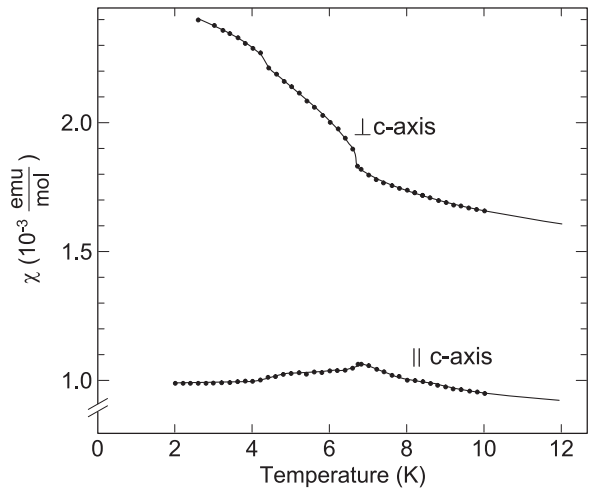

Figure 21. Temperature dependence of the bulk magnetic susceptibility of UPd_3. Note the small anomalies at T_0, T_1 and T_2 (data provided by McEwen).

The bulk magnetic susceptibilities $\chi_b^{\parallel,\perp}$ show relatively small anomalies at T_1 and T_2 and no noticeable change at T_0 (see figure 21), and also the overall variance of $\chi_{\rm bulk}^{\parallel,\perp}$ between T_2

and T_0 is not dramatic. It may safely be assumed that the U-sublattice susceptibilities are not behaving much differently. In contrast, for example σ_1 for $\boldsymbol{H}_{\rm ext} \perp \boldsymbol{c}$ changes from roughly 0.15 μs^{-1} near T_0 to $\sim$0.55 μs^{-1} just below T_2, while the corresponding $\chi_\perp$ changes only from 0.018 to 0.027 emu mol^{-1}. Also the jumps of σ_1 at T_2 and T_1 are significantly larger than the jumps of $\chi^\perp_{\rm bulk}$. On the other hand $K_1^\perp$ displays a much smaller change than $\chi^\perp$. Similar observations can be made for $\boldsymbol{H}_{\rm ext} \parallel \boldsymbol{c}$. What is then the origin of the much enhanced σ_1 relative to $\chi^\perp_{\rm bulk}$? The spread in fields at the μ^+ must be related to inhomogeneously distributed dipole fields arising from the field induced moments on the U sites and/or the local conduction electron spin polarization generated as well by the field induced moments via the RKKY mechanism. Both contributions should scale with the strength of the induced moments. Inhomogeneously distributed fields may result from extrinsic effects, which we have already ruled out, from a modulated lattice distortion, associated with the quadrupolar order, or from a field induced antiferromagnetic (AFM) order in the antiferroquadrupolar state, involving primarily the quasi-cubic U sites [25]. The latter two possibilities have indeed been considered, but the lattice distortions are too small (c/a changes by only -6×10^{-5} [25]) to cause the observed line broadening, and the induced AFM order produces unique dipole and contact field at the possible μ^+ sites [36].

A hint that the dipolar field may not contribute to the line broadening stems from the relatively huge change of $\sigma_1^\perp$ across T_1; since the relevant dipolar coupling constant is a given value and $\chi^\perp_{\rm bulk}$ or the relevant sublattice $\chi^\perp$ changes only by a few per cent, the change of $\sigma_1^\perp$ must have another origin.

The almost only remaining possibility is that the line broadening is associated with the contact hyperfine field, which implies that the conduction electron spin polarization is not the same at the involved μ^+ sites. In the light of the previous discussion this is not unexpected if again the effect of a non-spherical charge distribution of the 4f electrons on the RKKY coupling is invoked. In the quadrupolar phase below T_1 (or T_0) the quadrupole moment may assume up to four different orientations [25, 26], and hence one may expect to find a distribution of contact coupling constants depending on the actual arrangements of the quadrupoles next to the μ^+. A quantitative analysis of the anomalous features in the Knight shifts and the relaxation rates is not available yet, mainly due to our ignorance concerning the magnetic response of the two U sublattices, but it should be noted that $K_1^\parallel$ reveals a striking resemblance with the temperature dependence of the (1, 0, 3) resonance peak intensity in x-ray scattering (figure 3(a) of [26]).

3. Contact muon Knight shift in the presence of orbital s–f exchange

The aim of this section is to show that the accurate treatment of s–f exchange for CEF-split (LSJ) multiplet levels of the rare earth ion predicts, first, a temperature dependent amplitude $A^{\rm con}$ of the contact μ^+ Knight shift defined by

$$K_\alpha^{\rm con} = A^{\rm con} \cdot \chi(T)_\alpha, \tag{3.1}$$

and second, a variation of $A^{\rm con}$ in the case of a collective reorientation of the f-shell quadrupole moments. (Here α is a crystal symmetry axis and χ_α ($\equiv \chi_{\alpha\alpha}$) is the bulk susceptibility along this direction.) One will see that $A^{\rm con}$ consists of two terms

$$A^{\rm con} = A_0^{\rm con} + A_1^{\rm con}(T), \tag{3.2}$$

where $A_0^{\rm con}$ is the 'textbook' constant [47] derived from the usual isotropic exchange operator, and $A_1^{\rm con}$, the result of the contribution of the orbital exchange mechanism, is T-dependent and varies with the reorientation of the ionic quadrupoles. To show this, formulae for the exchange scattering including orbital processes [48–51] will be revisited and discussed in relation to the Knight shift.

In most metals, the measured $K_\alpha^{\rm con}(T)$ is in fact fairly well proportional to $\chi_\alpha(T)$, with $A^{\rm con} = A_0^{\rm con}$ determined by parameters ($k_{\rm F}$, etc) of the s-band and the distance of the test particle (nucleus, μ^+) from the magnetic ions. Temperature dependent $A^{\rm con}$ have however also been observed, namely in rare earth and actinide compounds, by NMR [54, 55, 31, 53] and by μSR. This 'anomalous' behaviour can have different origins; here the anisotropic exchange mechanism will be considered in the presence of a CEF.

The s–p spin polarization is the result of the exchange interaction $\propto \mathbf{s}\cdot\mathbf{s}_{{\rm f}p}$ between s-electrons and the pth ($p = 1, 2, \ldots, N$) f-electron with spins $\mathbf{s}$ and $\mathbf{s}_{{\rm f}p}$. The matrix element of the s–f exchange operator $H_{\rm ex}$ is often written in the 'isotropic' or de Gennes' form

$$\langle \mathbf{k}'\alpha'; JM_J'|H_{\rm ex}|JM_J;\mathbf{k}\alpha\rangle = -2\cdot I(k',k)\cdot(g_J-1)\langle JM_J'|\mathbf{J}|JM_J\rangle\langle\alpha'|\mathbf{s}|\alpha\rangle, \tag{3.3}$$

where $\boldsymbol{J}$ is the total angular momentum, $|JM_J\rangle$ are states of the f-shell, $|\mathbf{k},\alpha\rangle$ is an s-electron state with wavenumber $\mathbf{k}$ and spin α, and the dependence on $\mathbf{k}$, $\mathbf{k}'$ appears merely by the factor $I(k',k)$ (the results are similar by assuming $I = I(|\mathbf{k}'-\mathbf{k}|)$).

Equation (3.3) leads, for a weak (as compared to the LS-coupling) CEF, to a *temperature independent, isotropic* $A^{\rm con}$. In fact, for CEF-split terms Γ, Γ', ... within a given J manifold with states labelled by $|\Gamma\lambda\rangle$,

$$|\Gamma\lambda\rangle = \sum_{M_J} a(M_J)^{\Gamma\lambda}|M_J\rangle \tag{3.4}$$

a straightforward calculation [47] leads to an s-electron spin polarization at r_μ

$$(\rho_\uparrow - \rho_\downarrow)_\alpha = \sum_i^{\rm ions} f(k_{\rm F}r_{\mu i})\cdot I^*\cdot\langle\Gamma\lambda|J_\alpha|\Gamma\lambda\rangle. \tag{3.5}$$

Here $I^* = I^*(k_{\rm F})$ is an average value for $I(k',k)$ and f an oscillatory function with decreasing amplitude, and $\mathbf{r}_{\mu i} = \mathbf{r}_\mu - \mathbf{R}_i$ is the vector pointing from the ion at $\boldsymbol{R}_i$ to the muon (dealing with identical ions, the index i is dropped for $\boldsymbol{J}$). In a magnetic field $\boldsymbol{B}$ along the axis α, the thermal average of equation (3.5) over the states $|\Gamma\lambda\rangle$ leads to $\langle J_\alpha\rangle \propto \chi_\alpha(T)\cdot B$, and thereby to

$$K_\alpha^{\rm con}(T) = C\cdot\left(\sum_i^{\rm ions} f(2k_{\rm F}r_{\mu i})\right)\cdot I^*\cdot\chi_\alpha(T), \tag{3.6}$$

where $C = C(\mu_{\rm B}, k_{\rm F}, \ldots)$ is a constant.

A temperature dependent $K_\alpha^{\rm con}/\chi_\alpha = A^{\rm con}$ indicates, therefore, a physical situation where the *limited validity* of equation (3.3) becomes apparent. As shown by [48], de Gennes' formula equation (3.3) holds if

(1) all *accessible* states of the f-shell at the given T belong to a single J, and
(2) the 'orbital exchange mechanism', allowing in particular the change of the *orbital magnetic quantum numbers* in the $|LM'\rangle$, $|LM\rangle$ components of the states $|JM_J'\rangle$, $|JM_J\rangle$, can be neglected.

As to (1), it may be even at low temperatures not satisfied, when the CEF is sufficiently strong to mix—unlike in equation (3.4)—wavefunctions with *different* Js into $|\Gamma\lambda\rangle$ [52]. This J-mixing was invoked to explain the observed T-dependence of $A^{\rm con}$ in some 5f compounds [53]. (For the particular case of the lowest levels of the rare earth ions, J-mixing in the crystal field is in most cases negligibly small [56].)

The fulfilment of condition (2) is generally even less granted. It was shown [49, 51] that, for lanthanide compounds, the first correction terms to equation (3.3) accounting for orbital exchange may be considerably large; moreover, they add *qualitatively new features*

to the indirect RKKY ion–ion exchange interaction (anisotropic coupling [49–51, 57, 58], interaction terms *quartic* in the operators J_α [49]).

As shown below, the same turns out to be true for the μ^+ Knight shift: the terms neglected in de Gennes' expression give rise to a *T-dependent* $A^{\rm con}$, that also varies with the orientation of the f-shell quadrupoles. This is seen by examining the complete $H_{\rm ex}$ [48] as adapted for CEF-split levels according to equation (3.4). (The formula is quoted for the case of a less than half-filled f-shell for simplicity, but the method [48] is generally valid.) Within a single J-manifold one has

$$\langle \mathbf{k}', \alpha'; \Gamma'\lambda'|\hat{H}_{\rm ex}|\Gamma\lambda; \mathbf{k}\alpha\rangle = -2 \sum_{M'_J M_J} a(M'_J)^{\Gamma'\lambda'*} a(M_J)^{\Gamma\lambda} \sum_{M' M M'_S M_S} \langle J M'_J|M' M'_S\rangle \times \langle M M_S|J M_J\rangle I_{M'M}(\mathbf{k}'\mathbf{k}) \langle M'_S|\hat{\mathbf{S}}|M_S\rangle \langle \alpha'|\hat{\mathbf{s}}|\alpha\rangle, \tag{3.7}$$

where $\langle J M_J|M M_S\rangle$ are Clebsch–Gordan coefficients and

$$I_{M'M}(\mathbf{k}'\mathbf{k}) = \sum_{\mu,\nu} \mathrm{d}^{M'M}_{\mu,\nu} J_{\mu,\nu}(\mathbf{k}', \mathbf{k}) \tag{3.8}$$

are orbital integrals; $d^{M'M}_{\mu\nu}$ are constants determined by the admixture of the one-electron orbitals $\phi_{3\mu}(\mathbf{r}) = R_{4\rm f}(r) Y_{3\mu}(\mathbf{\Omega})$ in the states $|LM\rangle$ (one has $\sum_\mu \mathrm{d}^{M'M}_{\mu\mu} = \delta_{M'M}$), and

$$J_{\mu\nu}(\mathbf{k}'\mathbf{k}) = \int \mathrm{d}^3 r \int \mathrm{d}^3 r'\, \phi^*_{3\mu}(\mathbf{r}) v^*_{\mathbf{k}'}(\mathbf{r}') \frac{e^2}{|\mathbf{r}' - \mathbf{r}|} v_{\mathbf{k}}(\mathbf{r}) \phi_{3\nu}(\mathbf{r}'), \tag{3.9}$$

where $v_{\mathbf{k}}(\mathbf{r})$ are the orbital wavefunctions in the conduction band. For the single f-electron in $Ce^{3+}(4f^1\ {}^2F_{5/2})$, for example, one has $d^{M'M}_{\mu\nu} = \delta_{M'\mu} \cdot \delta_{M\nu}$ so that equation (3.8) simplifies to $I_{M'M}(\mathbf{k}'\mathbf{k}) = J_{M'M}(\mathbf{k}'\mathbf{k})$.

The case $I_{M'M} = I(\mathbf{k}'\mathbf{k}) \cdot \delta_{M'M}$ means that the orientation (i.e. M and M') of the orbital components of the $|J, M_J\rangle$ states is irrelevant in the exchange process and, in particular, only terms with $\Delta M_J = \Delta M_S$ remain in equation (3.7). Then, with

$$I_{M'M}(\mathbf{k}'\mathbf{k}) = I(\mathbf{k}'\mathbf{k}) \cdot \delta_{M'M} = I(\mathbf{k}'\mathbf{k}) \langle LM'|LM\rangle \tag{3.10}$$

the sums over $M'M$ can be performed and $\langle M'_S|\mathbf{S}|M_S\rangle$ transforms into $\langle J M'_J|\mathbf{S}|J M_J\rangle = (g_J - 1)\langle J M'_J|\mathbf{J}|J M_J\rangle$, giving back de Gennes' formula. With M-dependent diagonal and non-zero off-diagonal $I_{M'M}$ terms, however, the admixture of the matrix elements $\langle M'_S|\mathbf{S}|M_S\rangle$ *does not result* in $\langle J M'_J|\mathbf{S}|J M_J\rangle$. In particular, non-zero $M' \neq M$ orbital terms mean that in $\Delta M_J = \Delta M + \Delta M_S$ both orbital and spin parts contribute and the two exchange processes are intricately mixed via the L–S coupling by equation (3.7). (The de Gennes' expression is exact only for an 'orbitally spherical' state with $L = 0$, as for the ${}^8S_{7/2}$ ground level of Gd^{3+}. Indeed, in contrast to the 4f and 5f compounds discussed in section 2, no anisotropy or anomalous temperature dependence of the contact contribution to the Knight shift has been reported.)

That $I_{M'M}(\mathbf{k}', \mathbf{k})$ *does* in general depend on both M' and M is seen by separating radial and angular variables in the Bloch functions,

$$v_{\mathbf{k}}(\mathbf{r}) = \sum_{lm} u^{lm}_{\mathbf{k}}(r) Y_{lm}(\mathbf{\Omega}_{\mathbf{r}}) \tag{3.11}$$

and also in $|\mathbf{r}' - \mathbf{r}|$ via its series expansion in spherical harmonics. Equation (3.9) becomes

$$J_{\mu\nu}(\mathbf{k}'\mathbf{k}) = \sum_{l,l'=0,1,2\ldots} \sum_{\tilde{l}} \sum_{m,m'} g(\mathbf{k}', \mathbf{k}; l'm', lm, \tilde{l}) \langle \nu|Q_3(lm, l'm'; \tilde{l})|\mu\rangle, \tag{3.12}$$

where $\tilde{l}$ runs from $\max(|3-l'|, |3-l|)$ to $\min(3+l, 3+l')$ and both $l+\tilde{l}$, $l'+\tilde{l}$ have to be odd, since [49]

$$\langle \nu | Q_3(lm; l'm'; \tilde{l}) | \mu \rangle = 4\pi \sum_{\tilde{m}=-\tilde{l}}^{\tilde{l}} \langle Y_{3\nu}, Y_{\tilde{l}\tilde{m}} Y_{lm} \rangle \langle Y_{3\mu}, Y_{\tilde{l}\tilde{m}} Y_{l'm'} \rangle, \tag{3.13}$$

and

$$g(\mathbf{k}', \mathbf{k}; l'm', lm; \tilde{l}) = \frac{e^2}{2\tilde{l}+1} \int \mathrm{d}r \int \mathrm{d}r'\, r^2 r'^2 R_{4\mathrm{f}}(r) R_{4\mathrm{f}}(r') u_{\mathbf{k}}^{lm}(r) u_{\mathbf{k}'}^{*l'm'}(r') (r_<^{\tilde{l}} / r_>^{\tilde{l}+1}). \tag{3.14}$$

For plane waves $v_{\mathbf{k}}(\mathbf{r}) \approx \mathrm{e}^{\mathrm{i}\mathbf{k}\mathbf{r}}$ one has

$$u_{\mathbf{k}}^{lm}(r) = 4\pi \mathrm{i}^l j_l(kr) Y_{lm}^*(\mathbf{\Omega}_{\mathbf{k}}) \tag{3.15}$$

showing how, for $l', l > 0$, $g(\mathbf{k}', \mathbf{k})$ and thereby $J_{\mu\nu}(\mathbf{k}', \mathbf{k})$ and $I_{M'M}(\mathbf{k}', \mathbf{k})$ depend on the orientations of $\mathbf{k}'$ and $\mathbf{k}$. (The convergence in equation (3.12) is generally ensured by the short-ranged radial functions $R_{4\mathrm{f}}(r)$: ($\overline{r_{4\mathrm{f}}^2} = 0.2$–$0.3$ Å^2) and $j_l(0) = \delta_{l,0}$.)

Only the $l', l = 0$ term gives (by $\langle \nu | Q_3(00; 00; \tilde{l}) | \mu \rangle = \delta_{\mu\nu}\delta_{\tilde{l},3}$) an *isotropic* exchange integral $J(k', k) \cdot \delta_{\mu\nu}$ independent of the orbital magnetic quantum numbers, and leads therefore via equations (3.8)–(3.10) to de Gennes' formula with $I(k'k) = 4\pi g(k'k; 00; 00; 3)$ and $u_{\mathbf{k}}^{00}(r) = j_0(kr)$ in the integrand of g.

Thus, so far as the *angular dependence of* $v_{\mathbf{k}}(\mathbf{r})$ *within the range of the radial f-functions* $R_{4\mathrm{f}}$ *is negligible*, the orbital exchange mechanism can be ignored [48]. Clearly, when the anisotropy of the s-band wavefunctions within the f-shell is significant, the exchange integral $J_{\mu\nu}$ should indeed depend on the relative orientation of the f-orbitals with respect to $\boldsymbol{k}'$, $\boldsymbol{k}$, that is on μ, ν, and $\mathbf{\Omega}_{\mathbf{k}'}$, $\mathbf{\Omega}_{\mathbf{k}}$. For $L > 0$, therefore, $H_{\mathrm{ex}} \propto \mathbf{J} \cdot \mathbf{s}$ is only a *first approximation*.

For plane waves the arguments in $j_l(kr)$ reach within the 4f shell the value of $k_{\mathrm{F}} r \approx 0.5$, and therefore the first $l + l' \neq 0$ terms like that with $l' = 0, l = 2$ are not particularly small [49]. This shows that, depending on the actual s-band functions, orbital exchange in 4f or 5f compounds can become important.

Separating de Gennes' expression one has

$$\langle \mathbf{k}'; \Gamma'\lambda' | \hat{H}_{\mathrm{ex}} | \Gamma\lambda; \mathbf{k} \rangle = -2\{ I_{k'k}(g_J - 1) \langle \Gamma'\lambda' | \hat{\mathbf{J}} | \Gamma\lambda \rangle + \langle \Gamma'\lambda' | \hat{\mathbf{F}} | \Gamma\lambda \rangle \} \cdot \hat{\mathbf{s}}, \tag{3.16}$$

with

$$\hat{\mathbf{F}} = \sum_{M'M=-L}^{L} \tilde{I}_{M'M}(\mathbf{k}'\mathbf{k}) \mathbf{F}_{M'M}, \tag{3.17}$$

where $\mathbf{F}_{M'M}$ operates in the space of the f-shell states,

$$\mathbf{F}_{M'M} = \sum_{M_S' M_S} |M' M_S'\rangle \langle M_S' | \mathbf{S} | M_S \rangle \langle M M_S| \tag{3.18}$$

and the quantities $\tilde{I}_{M'M}(\mathbf{k}', \mathbf{k})$ *differ* from $I_{M'M}$ of equation (3.8) in that the sum in the series expansion for the integrals $J_{\mu\nu}(\mathbf{k}'\mathbf{k})$, equation (3.12), contains only the 'anisotropic' terms with $l + l' > 0$.

The essential point is that $\boldsymbol{F}$ is *not* a vector (i.e. not $\propto \mathbf{J}$), even if the components F_α are related to S_α. In particular, with the off-diagonal $M'M$ terms transitions with $|\Delta M_J| = |\Delta M + \Delta M_S| > 1$ come also into play, in contrast to an 'isotropic' interaction $\propto \langle M_J' | \mathbf{J} | M_J \rangle$.

The calculation of even the first terms in $\boldsymbol{F}$ is not simple, especially for the case of more than one f-electron, and it requires a knowledge of $v_{\mathbf{k}}(\mathbf{r})$ in the compound in question; it is not

attempted here. On the other hand, the structure of equations (3.16) and (3.17) allows some *general* conclusions.

First, in the paramagnetic state with no applied field $\boldsymbol{B}$ the thermal average of both terms in equation (3.16) vanish by time inversion symmetry. By applying $\boldsymbol{B}$, non-zero average values appear both for $\boldsymbol{J}$ and $\boldsymbol{F}$, and for not too strong fields these are linear in B_α. The same algebra and integrations over $\boldsymbol{k}'$, $\boldsymbol{k}$ leading to equation (3.5) give, by using equations (3.16) and (3.17),

$$K_\alpha^{\mathrm{con}}(T) = C \cdot \left(\sum_i^{\mathrm{ions}} f(k_{\mathrm{F}} r_{\mu i}) \right) \cdot I^* \cdot \chi_\alpha(T) + \sum_i^{\mathrm{ions}} \sum_{M'M} C^{(1)}_{M'M} b_{M'M}(k_{\mathrm{F}}; \mathbf{r}_{\mu i}) \chi_{\mathrm{F};M'M;\alpha}(T), \tag{3.19}$$

where $C^{(1)}_{M'M}$ are constants and $\chi_{\mathrm{F};M'M;\alpha}(T)$ are 'F–J' response functions determining the linear term in the thermal average $\langle F_{M'M,\alpha} \rangle = \chi_{\mathrm{F};M'M;\alpha}(T) \cdot B_\alpha + \cdots$ (the structure of $\chi_{\mathrm{F};M'M;\alpha}$ in terms of the states $|\Gamma\lambda\rangle$ and levels E_Γ is similar to that of χ_α). The oscillatory functions $b_{M'M}$ arise, like $f(2k_{\mathrm{F}} r_{\mu i})$, in the perturbation calculation for $(\rho_\uparrow - \rho_\downarrow)$ through integrations over $\boldsymbol{k}'$, $\boldsymbol{k}$ with the functions $\tilde{I}_{M'M}(\mathbf{k}', \mathbf{k})$ in the integrands. However, because of the dependence of $\tilde{I}(\mathbf{k}', \mathbf{k})$ on the orientation of its arguments (equations (3.12)–(3.15)), the resulting $b_{M'M}$ functions depend not only on $r_{\mu i}$, but also on the *orientation* of $\boldsymbol{r}_{\mu i} = \boldsymbol{r}_\mu - \mathbf{R}_i$. Thus, the anisotropy in $(\mathbf{k}', \mathbf{k})$ of the exchange integrals results in an *anisotropic s-electron spin density distribution* around each of the completely or partially oriented f-shell ions.

Since the operator $\boldsymbol{F}$ is not proportional to $\boldsymbol{J}$, the temperature dependence of the second sum in equation (3.19) is different from $\chi_\alpha(T)$. Thus, the two terms in equation (3.19) give

$$K_\alpha^{\mathrm{con}}(T)/\chi_\alpha(T) = A_0^{\mathrm{con}} + A_1^{\mathrm{con}}(T), \tag{3.20}$$

with

$$A_1^{\mathrm{con}}(T) = \sum_i \sum_{M'M} C^{(1)}_{M'M} b_{M'M}(k_{\mathrm{F}}; \mathbf{r}_{\mu i}) \chi_{\mathrm{F};M'M;\alpha}(T)/\chi_\alpha(T). \tag{3.21}$$

For temperatures $T \gg E_{\Gamma'} - E_\Gamma$ the response functions have the asymptotics $\chi_{\mathrm{F};M'M;\alpha}(T) \propto 1/T$ like $\chi_\alpha(T)$, and in this limit one has $A_1^{\mathrm{con}} \to$ const, as the data in section 2 indeed show.

Anisotropic exchange was invoked earlier [31] to explain the observed T-dependent $K_\alpha(T)/\chi_\alpha(T)$ in the NMR spectra of $CeAl_2$. A level-dependent hyperfine parameter was introduced, a phenomenological model to represent the variation described by equations (3.20) and (3.21).

A basic property of A_1^{con} is that, due to the above discussed anisotropy of the $b_{M'M}(\mathbf{r}_{\mu i})$ functions in equation (3.21), its value depends on a possible common orientation of the f-shells. Rotating this by applying a field $\boldsymbol{B}$ (in the case of, say, cubic symmetry), the first term in equation (3.19) does not change, both χ_α and $A_0 \equiv A_0^{\mathrm{con}}(r_{\mu i})$ being isotropic. In the second term $\propto A_1^{\mathrm{con}}$, however, the orientation of each of the f-shells relative to the position vectors $\mathbf{r}_{\mu i}$ does change, resulting in a variation of the Knight shift.

In HoB_2C_2 the term $A_1^{\mathrm{con}}(T)$ becomes conspicuous below $\approx$150 K (see figures 6, 7), accentuated by the small A_0^{con} at the μ^+ site. The particular dependence of A_1 on the direction of $\boldsymbol{B}$, having as *reference axis* the vector $\mathbf{r}_\mu - \mathbf{R}_{nn}$ pointing to the nearest neighbour ion (see figure 7), may simply reflect the fact that the spatial anisotropy of the s-polarization, for this special μ^+ site with a *single* nearest Ho^{3+}, is prevalently determined by this ion alone. Further, the AFQ ordering in this compound may suggest that the increasingly large A_1 on lowering T is in direct relation with a partial 'freezing out' of the quadrupolar degree of freedom in the paraquadrupolar phase. Assume for example that the lowest CEF state is the singlet $|\mathrm{S}\rangle$ coming from a Γ_4 or Γ_5 term split in the tetragonal field, the first excited states being the components $|\pm\rangle$ of the doublet. Then $\langle Q_{zz} \rangle_S = -2\langle Q_{zz} \rangle_\pm$ and the thermal average will deviate from zero

for low temperatures, $T \leqslant (E_D - E_S)$. Since these are also the temperatures where $A_1^{\rm con}(T)$ deviates from its asymptotical $\propto 1/T$ behaviour, a correlation between $\langle Q_{zz}\rangle$ and $A_1^{\rm con}(T)$ is not surprising.

A variation of $A_1^{\rm con}$ with the *reorientation of the quadrupole moments* should become easily observable when the ionic sites have a high (cubic or tetragonal) symmetry and some of the low lying Γ levels allow free rotation of the quadrupoles. The high symmetry is removed either by a transition to an ordered FQ or AFQ phase, or by an applied field $\boldsymbol{B}$ introducing a preferred orientation. On rotating $\boldsymbol{B}$, e.g. in the paraquadrupolar phase of CeB_6, the orientation of the quadrupole moments follows the corresponding rearrangement of the ionic eigenstates. Depending on the field strength, $\boldsymbol{B}$ leads to a quadrupole reorientation also below the ordering temperature [42, 59]. This does not affect $A_0^{\rm con}$, since the de Gennes' operator $\propto \mathbf{J}\cdot\mathbf{s}$ encodes all dependence of $K^{\rm con}$ on (Γ, λ) entirely into the variation of χ but, as discussed above, the reorientation becomes apparent in $A_1^{\rm con}$ (equation (3.21)). This is manifest in the case of CeB_6 (see figure 10, section 2) both in the paraquadrupolar and AFQ states, with the marked change of $A_1^{\rm con}$ in phase and amplitude for both μ^+ sites at $T_{\rm Q}$, as expected.

In the case of quadrupolar ordering, $A_1^{\rm con}$ should reflect the variation of the order parameter also through the corresponding changes in $v_{\mathbf{k}}(\mathbf{r})$. A full or partial ordering on the f-ion sublattice modifies the lattice potential $V(\mathbf{r})$ determining the s-band wavefunctions, and $v_{\mathbf{k}}(\mathbf{r})$ should sensitively change precisely in the f-shell regions, where the *anisotropic*, $l \neq 0$ components $u_{\mathbf{k}}^{lm}(r)Y_{lm}(\boldsymbol{\Omega}_{\mathbf{r}})$ of $v_{\mathbf{k}}(\mathbf{r})$ contribute to the exchange integrals $I_{M'M}$. This is particularly clear for OPW Bloch functions, orthogonal to the cores *and to the common f-state* of the ions on the ordered sublattices of an FQ or AFQ phase. The quadrupolar order parameter thereby enters $I_{M'M}(\mathbf{k}'\mathbf{k})$ and the quantities $b_{M'M}(\mathbf{r}_{\mu i})$ derived from them, modifying $A_1^{\rm con}$ via equations (3.17)–(3.19).

Lowering the temperature through $T_{\rm Q}$, the transition to a quadrupolar-ordered (FQ or AFQ) phase implies discontinuities in both $\chi(T)$ and the responses $\chi_{{\rm F};M'M}(T)$, consequently also in $A_1^{\rm con}(T)$. The discontinuity should affect the values or only the derivatives of $A_1^{\rm con}$ depending on the order of the phase transition. For CeB_6 the variation of $A_1^{\rm con}$ confirms that the transition is of second order.

The above discussion aimed at clarifying how orbital exchange scattering provides the possibility to observe quadrupolar order and its variation by the μ^+ implanted at the *interstitial* site $\mathbf{r}_\mu$. It is obvious, however, that the s-electron spin density, carrying over the information on the state of the ionic multipoles into the interstitial space, is strongly perturbed near $\mathbf{r}_\mu$ by the charged μ^+. The main consequence of this perturbation is that it *amplifies* the spin polarization, so that the corresponding 'enhancement factor' [37] enlarges the sensitivity of the μSR method. On the other hand, the orbital integrals may also change in the neighbourhood of the muon, an additional modification of $A_1^{\rm con}$ depending on the f-shell orientation with respect to $\mathbf{r}_{\mu i}$.

4. Interplay of quadrupolar and magnetic order

An interesting aspect of multipolar order is to what extent the different multipole components interact with each other, and which order parameter may be considered as primary, and which are of a secondary nature. Another phenomenon that might be monitored by μSR is the field induced antiferromagnetism within the quadrupolar ordered state. In the following we discuss results obtained in $PrCu_2$, CeAg, CeB_6 and $Ce_{0.75}La_{0.25}B_6$, UPd_3 and in the very recently investigated compound $DyPd_3S_4$.

4.1. $PrCu_2$

As mentioned in the introduction, $PrCu_2$ is known to show a combined nuclear-electronic order below ∼50 mK [5]. Hence it was a real surprise when ZF-μSR measurements revealed the

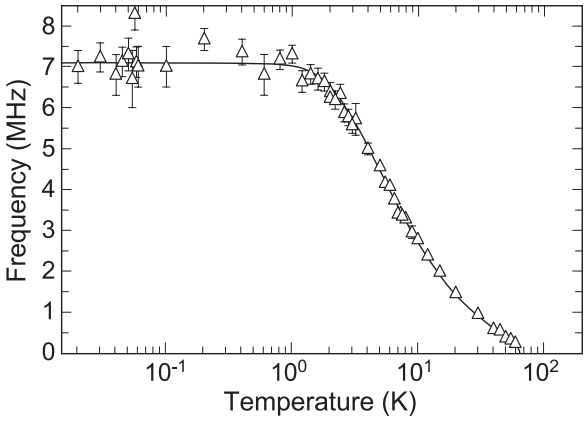

Figure 22. Temperature dependence of the spontaneous precession frequency in $PrCu_2$. The solid curve is a fit of equation (4.1) to the data (from [44]).

presence of a spontaneous internal field up to ∼65 K, displaying a very unusual temperature dependence [44]. The temperature dependence of the single spontaneous frequency is displayed in figure 22. It can be perfectly fitted by the expression

$$\nu(T) = \nu_0 \left[1 - \exp\left(\frac{-E}{kT}\right)\right]\left(1 - \frac{T}{T_{\rm cr}}\right)^{\beta} \tag{4.1}$$

with $E = 5.15 \pm 0.05$ K, $\beta = 0.38 \pm 0.04$ and $T_{\rm cr} = 64 \pm 2$ K. It is further found that the internal field $\boldsymbol{B}_\mu$ is strictly confined to the (a, c)-plane and encloses on average an angle θ with the a-axis which increases from ∼30° at 2 K to 45° at 20 K and then back to ∼35° at 55 K [44]. A particular $\boldsymbol{B}_\mu$ at a particular site may enclose an angle with the a-axis which could vary between −90° and +90°. The findings are not inconsistent with the incommensurately modulated structure below 50 mK determined by neutron diffraction (the ordered moments are also confined to the (a, c)-plane) and imply an ordered moment of 0.3 $\mu_{\rm B}$ for $T \to 0$ K. This value is smaller than the value from the neutron work: 0.54 $\mu_{\rm B}$. The quadrupolar ordering temperature at 7.5 K is not reflected in $\nu(T)$. The properties of $\boldsymbol{B}_\mu$ (widespread in value, varying orientation within the (a, c)-plane) rule out that $\boldsymbol{B}_\mu$ is somehow induced by the presence of the μ^+ at the 4e site.

Equation (4.1) appears to be made up of two factors. The factor $(1 - T/T_{\rm cr})^{\beta}$ could reflect the order parameter and $(1 - \exp(-E/kT))$ some additional suppression of the spontaneous field. Comparing these factors with the temperature dependence of other parameters of $PrCu_2$ we found that the temperature dependence of the elastic constant C_{66} [8] is precisely reproduced by $(1 - \exp(-E/kT))$ with $E = 5.15$ K. This is shown in figure 23. The stars are calculated according to

$$C_{66}(T) = C_0 - A\left[1 - \exp(-E/kT)\right]. \tag{4.2}$$

They seem to track the data even better than the solid line, which represents a calculation [8]. In second-order perturbation theory

$$C_{66}(T) - C_0 = -Ng^2\chi_{xy}(T) \tag{4.3}$$

where $\chi_{xy}(T)$ is the strain susceptibility, N the number of ions per unit volume, and g the magneto-elastic coupling constant. $\chi_{xy}(T)$ is given by

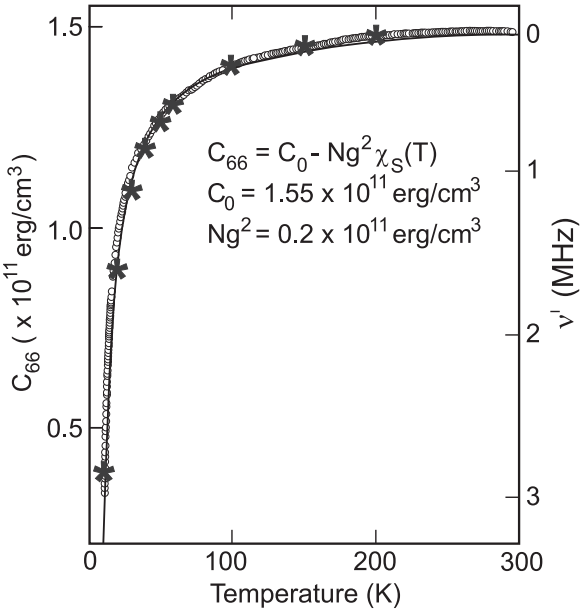

Figure 23. Temperature dependence of the elastic constant C_{66} in $PrCu_2$. The indicated stars are calculated with equation (4.2); see the text (from [44]).

$$\chi_{xy}(T) = \sum_{n\neq m} \frac{2|\langle n|O_{xy}|m\rangle|^2}{E_n - E_m} + \frac{1}{kT}\left\{\sum_n \frac{\exp(-E_n/kT)}{Z}|\langle n|O_{xy}|n\rangle|^2 - \left(\sum_n \frac{\exp(-E_n/kT)}{Z}\langle n|O_{xy}|n\rangle\right)^2\right\}. \tag{4.4}$$

$|n\rangle, |m\rangle$ are eigenstates of the crystalline-electric-field (CEF) Hamiltonian acting on the Pr^{3+} ground state multiplet $^3H_4$, E_n and E_m the corresponding eigenvalues, and $Z = \sum_n \exp(-E_n/kT)$ the partition function. O_{xy} is one of the quadrupole moment (Stevens) operators. As was shown in [8] and mentioned in the introduction, O_{xy} is also the relevant operator in the quadrupolar interaction responsible for the establishment of the ferroquadrupolar order below T_{JT}. Hence we may write for the ordered moment

$$\mu(T) = K\chi_{xy}(T)(1 - T/T_{cr})^{\beta}, \tag{4.5}$$

where K is some numerical constant. This empirical relation may lend itself to the following interpretation. The appearance of non-zero quadrupole expectation values causes strain which, via the magneto-elastic coupling by a kind of reversed magnetostrictive effect, induces the complex magnetic order that we have seen. The strain itself disappears above T_{cr}. This could mean again that below T_{cr} the degrees of freedom of the quadrupole moments are partially frozen out, establishing a semi-ordered quadrupolar state, while the fully ferroquadrupolar state is only established below T_Q. This view is supported by relaxation effects; see section 5. Note that T_Q is not reflected in $\nu(T)$. This indicates that the fully established ferroquadrupolar state below T_Q and the 'partial' quadrupolar order below T_{cr} are sufficiently 'similar' as not to alter the magnetic state. Note also that the magnetic state is not modified by a non-zero H_{ext} as follows from the splitting of the TF signal below T_{cr} for $\boldsymbol{H}_{ext} \parallel (a, c)$-plane [44].

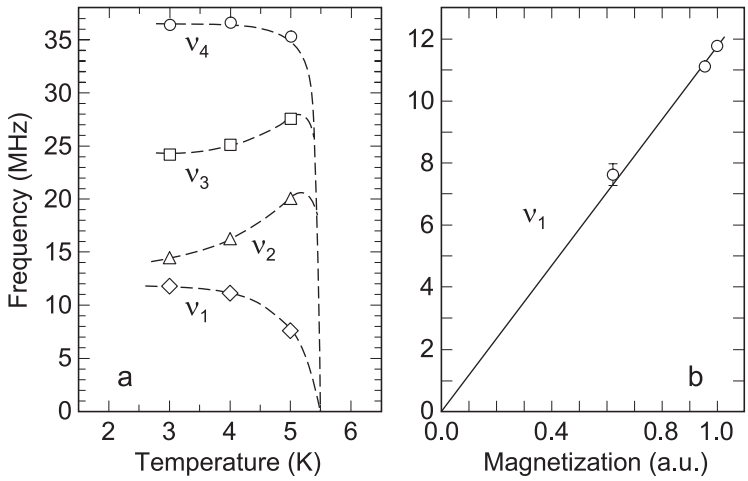

Figure 24. (a) Temperature dependence of the four spontaneous precession frequencies ν_i below T_c in CeAg, (b) plot of ν_1 versus the saturation magnetization (from [43]).

Of course, the question arises, why the high temperature magnetic order was not seen in the neutron scattering experiment. It is possible that the magnetic structure is too short ranged or highly irregular to be resolved by neutron diffraction. This view is supported by the observation that the inhomogeneity of the spontaneous internal fields is much larger than expected on the basis of the incommensurately modulated structure found below 50 mK. On the other hand, the inhomogeneity may be also caused by the random Pr nuclear dipole field enormously enhanced by the hyperfine-interaction-induced polarization of the f-electron shell [6, 44]. In summary, the invisibility of the high temperature magnetic order to neutrons is not yet fully understood. Currently attempts are under way to confirm the high temperature magnetic order by NMR measurements using the Cu nuclear spins. First encouraging results have been obtained [83].

4.2. CeAg

This compound is known to order ferromagnetically below 5.5 K. ZF-μSR measurements revealed four spontaneous frequencies ν_i whose temperature dependence is displayed in figure 24 [43]. The frequencies ν_2, ν_3, and ν_4 are attributed to μ^+ localized at the c site, and correspond to the threefold-split TF signal above T_c, discussed in section 2. The fourth frequency, ν_1, which scales very well with the domain magnetization M_d (see figure 24), is attributed to μ^+ localized at a defect site. As can be seen, the temperature dependence of ν_2, ν_3 and ν_4 is anomalous. In particular, ν_2 and ν_3 rise with increasing temperature on approaching T_c and do not follow $M_d(T)$.

For a ferromagnet with zero net magnetization the internal field is given by [60]

$$\begin{aligned} \boldsymbol{B}_i &= \frac{4\pi}{3}\boldsymbol{M}_d + \boldsymbol{B}_i^{dip} + \boldsymbol{B}_i^{con} \\ &= \frac{4\pi}{3}\boldsymbol{M}_d + \left(\overleftrightarrow{A}_i^{dip} + A_i^{con}\right)\cdot \boldsymbol{M}_d, \end{aligned} \tag{4.6}$$

where the first term represents the Lorentz field and $\boldsymbol{M}_d$ is the domain magnetization. According to [18] the ordered moments or $\boldsymbol{M}_d$ ($\simeq 1\ \mu_B$/Ce), respectively, are oriented along the c-axis, and therefore $\overleftrightarrow{A}_i^{dip} \cdot \boldsymbol{M}_d = A_{cc,i}^{dip} M_d$, where $A_{cc,i}^{dip}$ are given by the calculated values

Table 2. Compilation of spontaneous frequencies ν_i, internal fields B_i, extracted hyperfine fields at 3 K and considered site assignments.

Signal i	ν_i (MHz)	B_i (kG)	$B_{\rm dip} + B_c$ (kG)	B_c (kG)[a]	Site
1	11.79 (13)	±0.87 (7)	<u>+0.145</u>, −1.59	−0.64 (1)	Ag vacancy
2	14.47 (26)	±1.07 (22)	+0.345, <u>−1.795</u>	−0.30 (2)	$(0\frac{1}{2}\frac{1}{2})$
3	24.21 (7)	±1.79 (5)	+1.065, <u>−2.515</u>	−3.22 (1)	$(\frac{1}{2}0\frac{1}{2})$
4	36.42 (26)	±2.69 (22)	+1.965, <u>−3.415</u>	−4.20 (2)	$(\frac{1}{2}\frac{1}{2}0)$

[a] B_c is obtained by using the underlined values for $B_{\rm dip} + B_c$ and calculated $B_{\rm dip}$ for the considered site from table 1 and $\mu = 1\ \mu_{\rm B}$.

for the c sites (see section 2.4). The peculiar temperature dependence of $B_i(T)$ may then again be traced back to $A_i^{\rm con}(T)$, assuming that the ferromagnetically ordered moments in the vicinity of the μ^+ are not affected by the μ^+. A straightforward extraction of $A_i^{\rm con}(T)$ from equation (4.6) is impeded by the fact that the relative sign of $\boldsymbol{B}_i$ and $\boldsymbol{M}_{\rm d}$ is not determined in zero field measurements. The possible values of $(A_{cc,i}^{\rm dip} + A_i^{\rm con})M_{\rm d}$ at 3 K are collected in table 2. Independently of the choice of the sign of $\boldsymbol{B}_i$ $(i = 2, 3, 4)$ relative to $\boldsymbol{M}_{\rm d}$ and the assignment of the ν_i to a particular c site, we find that the contact coupling constant $A_i^{\rm con}$ has to rise with increasing temperature when $T_{\rm c}$ is approached in order to reproduce $\nu_i(T)$. A possible choice is to assign ν_2 to the site $(0\frac{1}{2}\frac{1}{2})$, ν_3 to $(\frac{1}{2}0\frac{1}{2})$ and ν_4 to $(\frac{1}{2}\frac{1}{2}0)$, and to assign a negative sign to B_2, B_3 and B_4. With this choice we extract the $A^{\rm con}$ values displayed in figure 14. $A^{\rm con}$ for the site $(0\frac{1}{2}\frac{1}{2})$ shows a smooth increase in absolute value from 3 K up to high temperatures. For the other two sites an abrupt change of $A^{\rm con}$ at $T_{\rm c}$ is indicated. Similar results are found for other choices, demonstrating that some of the contact coupling parameters are strongly modified by the ferromagnetic phase transition in contrast to the absence of any anomalies at $T_{\rm Q}$.

Hence it appears as if the ferroquadrupolar state undergoes some structural modification at $T_{\rm c}$. Between $T_{\rm c}$ and $T_{\rm Q}$ no evidence for static magnetic features are seen, either in zero field or in transverse fields.

4.3. CeB_6, $Ce_{1-x}La_xB_6$

Below $T_{\rm N} = 2.3$ K, CeB_6 develops a rather complicated antiferromagnetic structure characterized by a multiple-$\boldsymbol{k}$ behaviour [2]. As was pointed out before, the μ^+ occupy a unique site, the d site, in this cubic compound. Yet below $T_{\rm N}$ in zero field eight different spontaneous internal fields are observed (see figure 25) [61]. With the magnetic structure promoted in [2], it proved impossible to explain the presence of eight internal fields. Recent new neutron powder, single-crystal diffraction and spherical polarimetry measurements lead to a new structure determination (D model), which admitted the occurrence of eight different fields across the d sites [9]. However, to reproduce at least approximately also the values of the local fields, the contact coupling constants $A_{\parallel}^{\rm con}$ and $A_{\perp}^{\rm con}$ had to change from -4.2 and 2.3 kG/$\mu_{\rm B}$ just above $T_{\rm N}$ (see figure 8) to +4.4 and +1.67 kG/$\mu_{\rm B}$, respectively, for $T \to 0$ K. (Remarkably, the latter two values are closer to the values above $T_{\rm Q}$.) The anomalous temperature dependence of three out of the eight spontaneous frequencies, not reflected in the neutron data, may again be attributed to $A^{\rm con}$. It is interesting to note that in model D of [9] the in-plane arrangement of the magnetic dipole moment and the O_{xy}-type electrical quadrupole moments is the same, while this correspondence is lost when comparing neighbouring (001)-planes. Also the dipole moment values are different on neighbouring planes. It is suggested that, besides magnetic dipoles and electric quadrupoles, magnetic octupoles also play an important role, in particular stabilizing the magnetic moment arrangement in the D model [9].

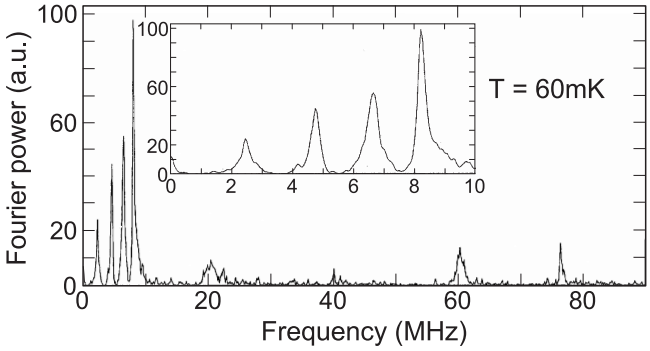

Figure 25. Fourier spectrum of the ZF-μSR signal in CeB_6 at 60 mK, showing the presence of eight spontaneous precession frequencies (from [61]).

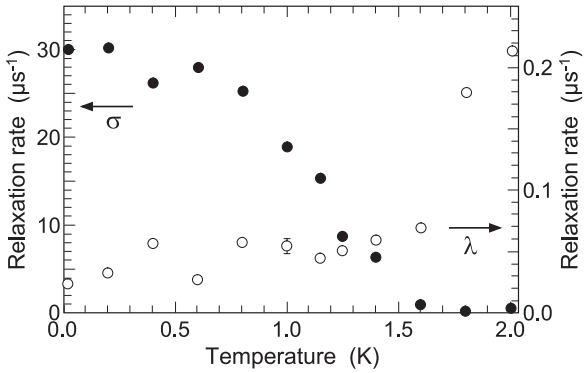

Figure 26. Temperature dependence of the Gaussian and exponential relaxation rates σ and λ in $Ce_{0.7}La_{0.3}B_6$. The ZF-μSR signal follows the expression $P(t) = A_1 \exp(-\sigma^2 t^2) + A_2 \exp(-\lambda t)$ with $A_2 \simeq A_1/4$ below $\sim$0.7 K (from [62]). The exponentially relaxing component, which indicates spin–lattice relaxation, signals the persistence of fluctuating field components in phase IV.

As mentioned in the introduction, below T_Q a field induced simple antiferromagnetic order is observed in CeB_6. This order leads to zero effective dipole and contact fields at the highly symmetric d site and hence cannot be seen by the muons. In fact no magnetic signature was seen in the TF measurements below T_Q, quite in contrast to NMR measurements involving the B-nuclei [12].

The magnetic and quadrupolar phase diagram of CeB_6 becomes more complicated by partial substitution of Ce by La. A new phase IV appears (see figure 3), the nature of which is not yet fully characterized and understood. Neutron scattering has not produced evidence for long range magnetic order in phase IV [15]. However, ZF-μSR measurements in samples with $x = 0.7$ [62] and $x = 0.75$ [63] show a rapidly increasing Gaussian relaxation behaviour when crossing into phase IV below $\sim$1.6 K. See figures 26, 27. Phase IV extends down to zero temperature for $x = 0.7$ and down to $\sim$1.3 K for $x = 0.75$. In the latter case phase III reappears below 1.3 K. The Gaussian relaxation rates imply static internal field spreads of the order of 300–500 G or randomly frozen moments of order 0.13–0.16 μ_B. This could indicate that a random static order similar to the order in a spinglass is established in phase IV, but certainly long range order is also ruled out by the μSR results. On the other hand, recent thermal expansion measurements in phase IV suggest that phase IV is characterized by a ferroquadrupolar order with $\langle O_{yz} \rangle = \langle O_{zx} \rangle = \langle O_{xy} \rangle \neq 0$ [64]. If true, it is

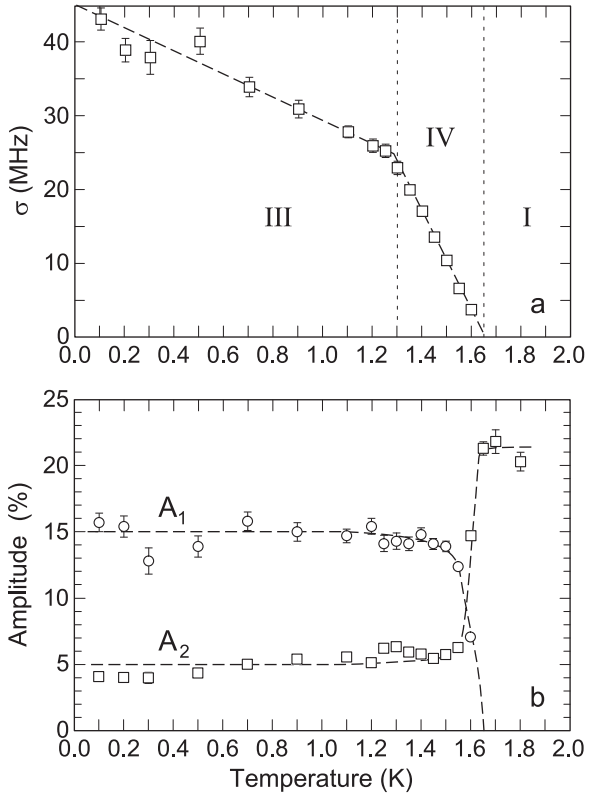

Figure 27. Temperature dependence of (a) the Gaussian relaxation rate σ and (b) the amplitudes A_1 and A_2 of the Gaussian and exponential components, respectively, in $Ce_{0.75}La_{0.25}B_6$. See the caption of figure 26. The extension of phase IV is clearly visible (dashed vertical lines). Note that the Gaussian component is absent in the paramagnetic phase (from [63]).

tempting to speculate that the random static order revealed by μSR is somehow connected to the ferroquadrupolar order, perhaps similar to the case in $PrCu_2$, a problem left for future studies. It has also been suggested that phase IV is characterized by magnetic octupolar ordering [3]. A resultant field of about 40 G is estimated for the d site which is clearly not supported by the measurements. This does not necessarily rule out octupolar order since the octupolar fields may be masked by dipolar fields.

Interestingly in the $x = 0.75$ sample below 1.3 K, i.e. in phase III, the dominant μSR signal is still showing a Gaussian relaxation instead of the multifrequency signal seen in CeB_6 in phase III [63]. The random field spread extrapolated to zero temperature amounts to 500 G, more or less equal to the result in the $x = 0.7$ sample [61]. However, the III–IV phase transition is well reflected in the slope $d\sigma/dT$. The absence of a multifrequency signal is puzzling, since recent neutron diffraction results show that the magnetic structures of phase III in CeB_6 and $Ce_{0.75}La_{0.25}B_6$ are apparently identical [15].

We hope to learn more about the nature of phase IV by further Knight shift measurements.

4.4. UPd_3

It is claimed that the phase transition at $T_2 \simeq 4.4$ K is partially of a magnetic nature, leading to a very weak antiferromagnetic order with limited correlation length and with very small

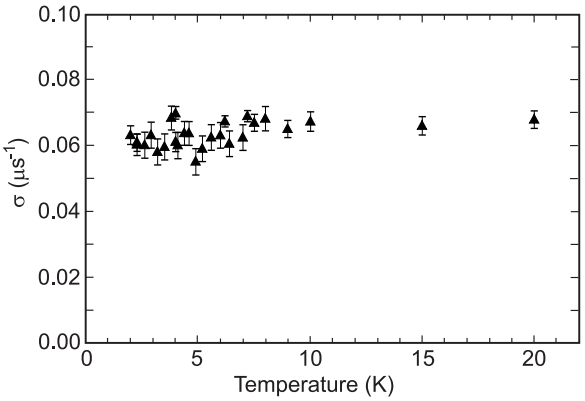

Figure 28. Temperature dependence of the ZF relaxation rate σ in UPd_3. Note the absence of any anomalies at either T_0, T_1 or T_2 (from [36]).

ordered moments of order 10^{-2} μ_B/U atom or less, and partially associated with changes in the antiferroquadrupolar (AFQ) order [24, 25]. ZF-μSR measurements below T_2 [36] showed the μ^+ polarization to follow a Kubo–Toyabe function with a rather small decay constant of $\sigma \simeq 0.065$ μs^{-1} (see figure 28). This value can be reproduced by considering only the nuclear dipole fields of the ^{105}Pd constituents. A moment as small as 0.01 μ_B on the quasi-cubic U sites would lead to internal fields of 2–26 G considering various possible μ^+ sites and simple antiferromagnetic structures. Such fields should have been well visible in the μSR spectra. For example, a random field of 2 G would lead to a decay rate of $\sigma = 0.17$ μs^{-1}, much larger than the observed value. The situation is reminiscent of the situation in UPt_3 [65–68] and was explained on the basis of slow AF-correlated spin fluctuations, which within the time window of neutron scattering appear static and within the time window of μSR appear fully dynamic [69].

The Knight shift K_1 drops remarkably below T_2 for $\boldsymbol{H}_{ext} \perp c$-axis (see figure 20) and appears rather temperature independent for $\boldsymbol{H}_{ext} \parallel c$-axis (see figure 19). It is argued in [39] that this behaviour is again to be attributed to the contact hyperfine field and the local conduction electron polarization which is affected by the changes in the AFQ structure. Resonant x-ray scattering on UPd_3 has revealed directly the change in AFQ structure at T_1 [26], but corresponding results for the change at T_2 are not yet available.

4.5. $DyPd_3S_4$

We recall that this compound shows two magnetic phase transitions at $T_{N_1} \simeq 1$ K and $T_{N_2} \simeq 0.75$ K and an antiferroquadrupolar transition at $T_Q = 3.4$ K. So far only results from powder samples are available. Preliminary μSR measurements in zero and longitudinal fields reflect all three phase transitions; see figure 36 [70]. Below T_{N_1} the ZF as well as the LF signal at 0.1 T is best fitted by the three-component function

$$P(t) = A_1 e^{-\frac{1}{2}\sigma^2 t^2} + A_2^{-\lambda_2 t} + A_3 e^{-\lambda_3 t} \tag{4.7}$$

with $A_2 + A_3 \simeq \frac{1}{2}A_1$. Above T_{N_1} in ZF, $P(t)$ changes to the two-component function

$$P(t)_{ZF} = A_1' e^{-\lambda_1' t} + A_2' e^{-\lambda_2' t} \tag{4.8}$$

and in LF up to T_Q to

$$P(t)_{LF} = A_1^* e^{-\frac{1}{2}\sigma^{*2} t^2} + A_2^* e^{-\lambda_2^* t}. \tag{4.9}$$

The latter observation is quite uncommon, since usually in LF the μ^+ spin is more or less decoupled from static internal fields and the observed relaxation is of the spin–lattice relaxation type and follows an exponential behaviour. Interestingly σ^* has the same magnitude as σ below T_{N_2}. This could suggest that the external field induces a magnetic order below T_Q as observed in CeB_6 and other compounds, and that this order is the same as in ZF below T_{N_2}. Indeed subsequent neutron diffraction studies at PSI have confirmed this conjecture [70]. The μSR data present several puzzles, which have to be understood in the future. For example, the amplitudes above T_{N_1} are more or less the same in ZF and LF, but are temperature dependent, i.e. $A_1' \simeq A_1^*$ and $A_2' \simeq A_2^*$. (Note that $\sum_{i=1}^{2} A_i' = \sum_{i=1}^{2} A_i^* = A_{tot}$, where A_{tot} is the total asymmetry, as obtained by calibration measurements in weak TF above T_Q. Hence all implanted μ^+ contribute to the μSR signal.) A $\sigma \simeq 80\ \mu s^{-1}$ translates into a field spread of $\sim$940 G, comparable to the applied field. Therefore on the basis of the Kubo–Toyabe scenario one would have expected that $A_1^* < A_1$. At 0.9 K one finds even that $A_1^* > A_1$. Further features will be discussed on section 5.

5. Dynamic effects

5.1. Introduction

As far as we are aware of little is known about the interplay of quadrupolar degrees of freedom and f-electron spin dynamics. Since f-electron magnetic dipole moments and electric quadrupole moments are not independent of each other, it may be expected that the development of quadrupolar order could be reflected in a slowing down of the spin dynamics and a consequently increased spin–lattice relaxation rate of the implanted μ^+. The fluctuating magnetic fields at the μ^+ arise, as in the static case, either directly from the 4f-moments or indirectly via the induced conduction electron spin polarization. In the latter case random stochastic reorientations of the quadrupole moment may also render the RKKY coupling time dependent and contribute to the fluctuations of the conduction electron spin polarization at the μ^+, i.e. the fluctuations arise from the fluctuating f-moments, $\boldsymbol{\mu}_f(T)$, and from the stochastic time dependence of the exchange integral in the RKKY mechanism. Hence within the frame of the Redfield theory [71] we may write for the μ^+ spin–lattice relaxation rate

$$\lambda = \frac{1}{T_1} = \gamma_\mu^2 \langle B_{dip}^2 \rangle \frac{\tau_{dip}}{1 + \omega^2 \tau_{dip}^2} + \gamma_\mu^2 \langle B_c^2 \rangle \frac{\tau^*}{1 + \omega^2 \tau^{*2}}, \tag{5.1}$$

with

$$\frac{1}{\tau^*} = \frac{1}{\tau_{dip}} + \frac{1}{\tau_Q}, \tag{5.2}$$

where τ_{dip} and τ_Q are correlation times characterizing the 4f dipole- and quadrupole-moment fluctuations, respectively. $\langle B_{dip}^2 \rangle$ and $\langle B_c^2 \rangle$ are the second moments of the corresponding field distributions in the static case and $\omega = \gamma_\mu H_{ext}$.

We have indeed found that the μ^+ spin–lattice relaxation rate λ is affected by the onset of quadrupolar order in $PrCu_2$, CeAg and $DyPd_3S_4$; see below. In UPd_3, λ was unmeasurably small. In CeB_6, λ was large enough to be measured, but no significant anomaly at or near T_Q was visible [72]. According to [72] the observed temperature dependence of λ in a small longitudinal field above T_Q is predominantly caused by the Kondo effect, involving the d-type conduction electrons.

In the quadrupolar ordered phase one may also expect to see collective excitations, analogous to magnon excitations; see e.g. [73, 74]. This may lead to characteristic temperature

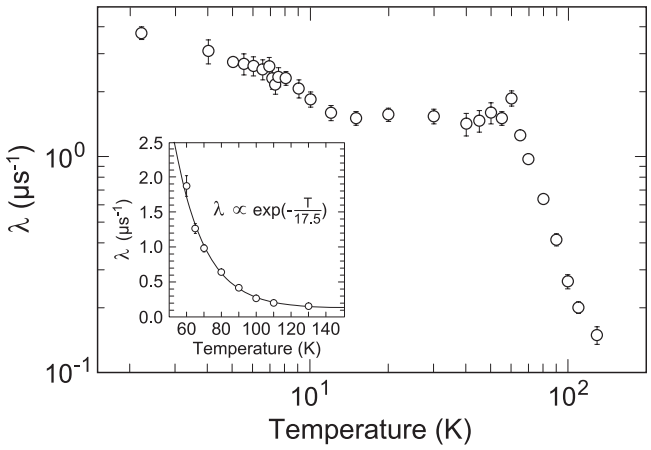

Figure 29. Temperature dependence of the spin–lattice relaxation rate λ in ZF in $PrCu_2$. The inset shows λ above 60 K; the solid curve represents an exponential fit (from [44]).

dependences in the μ^+ relaxation rates (as observed in the case of magnon excitations), which may be observable. This possibility needs still to be explored.

5.2. $PrCu_2$

The zero field measurements revealed that the non-oscillating component of the initial μ^+ polarization along the spontaneous internal field displayed significant relaxation and above $T_{cr} \simeq 64$ K the full initial polarization relaxed [44]. The results are shown in figure 29. As can be seen, a cusp-like behaviour appears at T_{cr} and above T_{cr} λ decreases exponentially with rising temperature (see the inset). However, no anomaly is evident at the quadrupolar ordering temperature $T_Q \simeq 7.5$ K. The increase of λ on approaching T_{cr} from above seems to signal a slowing down of the field fluctuations at the μ^+, preceding the appearance of the 'high temperature' magnetic order, as described in the previous section. Upon application of a longitudinal field $\lambda(T)$ is reduced, most strongly near T_{cr}, and the cusp tends to be rounded off. Above a field of 400 Oe the anomaly near T_{cr} has disappeared (see figure 30, showing λ at 2 kOe), and $\lambda(T)$ is well fitted by the expression (except in the vicinity of T_Q)

$$\lambda^*(T) = \frac{\lambda_0}{T} + \lambda_{const}, \tag{5.3}$$

where λ_0 is strongly anisotropic, while $\lambda_{const} \simeq 0.095\ \mu s^{-1}$ is independent of orientation. Interestingly the data show a cusp-like anomaly at T_Q which grows with the strength of the applied field (see the inset in figure 30). In summary, the ZF data display an anomaly at T_{cr}, but not at T_Q, while in strong LF an anomaly appears at T_Q, but not at T_{cr}. The field dependence of λ has been measured at various temperature up to 80 K for both $\boldsymbol{H}_{ext} \parallel \boldsymbol{c}$ and $\boldsymbol{H}_{ext} \parallel \boldsymbol{b}$. The results for $\boldsymbol{H}_{ext} \parallel \boldsymbol{c}$ are displayed in figure 31. The data can be well fitted by the equation

$$\lambda(T, H) = \frac{\gamma_\mu^2 \langle \widetilde{B}_\perp^2 \rangle \tau_c(T)}{1 + \omega^2 \tau_c^2} + \lambda^*(T), \tag{5.4}$$

involving a field dependent and a field independent term. The latter is precisely given by equation (5.2) and the first term by the Redfield formula. The fitted values of the parameters τ_c, $\gamma_\mu^2 \langle \widetilde{B}_{\perp,2}^2 \rangle$ and λ^* are displayed in figure 32 as a function of temperature.

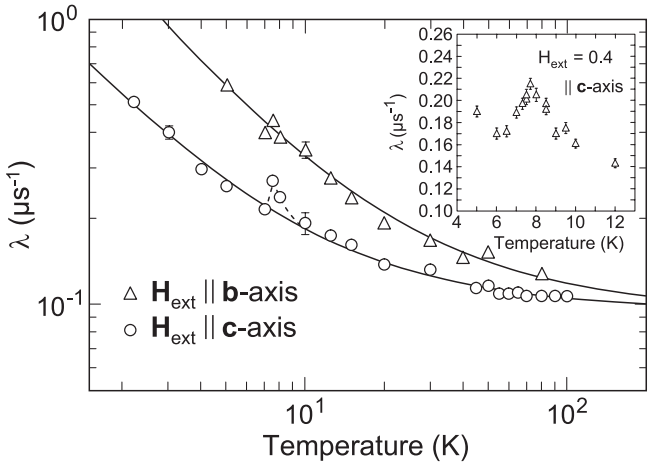

Figure 30. Temperature dependence of λ in LF at 2 kOe for $\boldsymbol{H}_{\rm ext} \parallel b$-axis and for $\boldsymbol{H}_{\rm ext} \parallel c$-axis in $PrCu_2$. The solid curves represent fits of equation (5.2) to the data. The inset show λ at 4 kOe, displaying a pronounced cusp at $T_{\rm Q} = 7.5$ K (from [44]).

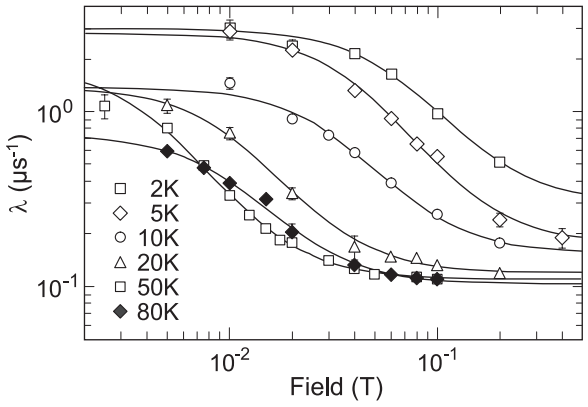

Figure 31. Longitudinal field dependence of λ in $PrCu_2$ at various temperatures for $\boldsymbol{H}_{\rm ext} \parallel c$-axis. The solid curves are fits of equation (5.3) to the data (from [44]).

We now first discuss the field independent term. The field independence implies that $\omega\tau_c^* \ll 1$, where τ_c^* is the relevant correlation time of the responsible fluctuating fields $\widetilde{B}_\perp^*$ and hence $\tau_c^* \ll 1/\omega = 1/\gamma_\mu H_{\rm ext}$ up to at least $H_{\rm ext} = 4$ kOe, i.e. $\tau_c^* \ll 3 \times 10^{-9}$ s. With $\lambda^*(2\ {\rm K}) \simeq 1\ \mu{\rm s}^{-1}$ for $\boldsymbol{H}_{\rm ext} \parallel \boldsymbol{c}$ it follows that $\sqrt{\langle \widetilde{B}_\perp^{*2} \rangle} \gg 1.35$ kG. Both the short τ_c^* and the large fluctuating field amplitude indicate that one seems to monitor fluctuations of an appreciable part of the full Hund's rule moment of Pr^{3+} (3.58 $\mu_{\rm B}$). The anisotropy of λ_0, i.e. $\lambda_0(\boldsymbol{H}_{\rm ext} \parallel \boldsymbol{b})/\lambda_0(\boldsymbol{H}_{\rm ext} \parallel \boldsymbol{c}) \simeq 4$, implies that the fluctuating fields are well confined to the (a, c)-plane and within the (a, c)-plane nearly perpendicular to the static spontaneous fields below $T_{\rm cr}$. The absence of any anomaly at $T_{\rm cr}$ (no slowing down of the spin dynamics upon approaching $T_{\rm cr}$ from above) implies that only a small fraction of the full Hund's rule moment is involved in the magnetic order below $T_{\rm cr}$, as already indicated by the small ordered moment of $\sim$0.29 $\mu_{\rm B}$ below 1 K. However, it is remarkable that the onset of the antiferroquadrupolar order at $T_{\rm Q}$ leads to an increase of λ^*, which indicates that the fluctuations are slowed down

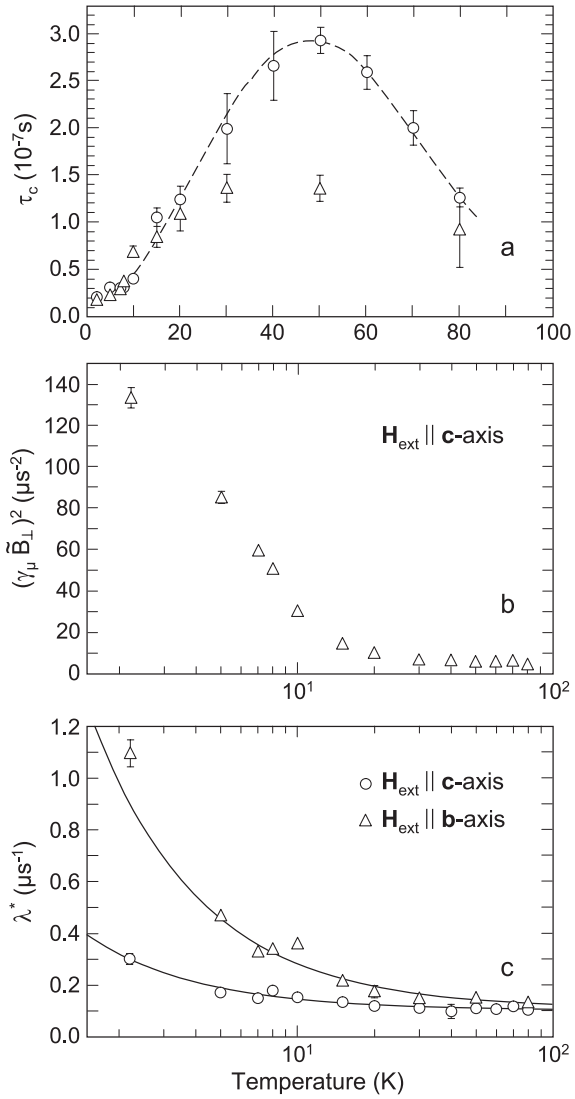

Figure 32. Temperature dependence of (a) τ_c, (b) $(\gamma_\mu \tilde{B}_\perp)^2$, (c) λ^* in $PrCu_2$. The solid curve in (c) represent fits of equation (5.2) (from [44]).

by perhaps 30% at and near T_Q. This feature, limited to a region close to T_Q, needs still to be analysed. The overall $1/T$ dependence translates into $\tau^* \propto T$, which suggests that the 4f electron relaxation is basically induced by the Korringa mechanism.

Next we turn to the field dependent contribution to λ, the first term in equation (5.3). Figures 32(a), (b) display a rather unusual behaviour. The fluctuation rate $1/\tau_c$ is relatively slow, amounting to 5×10^7 s^{-1} at $\sim$2 K, decreases to a minimum of 3×10^6 s^{-1} at 50 K, and starts to increase again above 50 K. In comparison to $1/\tau_c^*$, $1/\tau_c$ is at least an order of magnitude slower. Very unusual is the temperature dependence of the involved fluctuating field amplitudes $\widetilde{B}_\perp$, which are essentially isotropic and drop rapidly from about 140 G at 2 K to less than 10 G above 20 K. From the ratio $\widetilde{B}_\perp/\widetilde{B}_\perp^*$ one estimates that the slowly fluctuating moment components are of order 0.1 μ_B at 2 K.

We are thus confronted with a situation in which the Pr 4f-moment possesses a large anisotropic component which fluctuates rapidly, perhaps driven by the Korringa mechanism, and a small slowly relaxing, essentially isotropic component which slows down when T_{cr} is approached from above and splits into a static part below T_{cr}, manifest through the spontaneous static field, sensed by the μ^+, and a component which continues to generate fluctuating fields at the μ^+. As figures 32(a), (b) imply, the latter components gain in strength and the fluctuation rate increases as the temperature is decreased.

Following the assertion, promoted in section 4, that the spontaneous magnetic order is driven by a primarily quadrupolar mechanism, we also consider that the slowing down observed in ZF, preceding the establishment of the 'high temperature' magnetic order, is somehow connected to quadrupolar effects, and it appears reasonable to assume that it reflects the freezing out of quadrupolar degrees of freedom which also controls the slowing down of a part of the full Hund's rule moment of Pr^{3+}. The persisting slow and unusual spin dynamics below T_{cr} (besides the fast component) may be attributed to the remaining degrees of freedom of the quadrupole and the relevant dipole moments. The increase of $\widetilde{B}_\perp$ below 20 K (see figure 32(b)) may reflect the increase of $A^{con}_{a,b}$ (see figure 18) and the peculiar temperature dependence of τ_c (figure 32(a)) may originate from different temperature dependences of τ_{dip} and τ_Q, with $\tau_{dip} < \tau_Q$ at low T and $\tau_{dip} > \tau_Q$ above T_{cr}. Hence the μ^+ relaxation above T_{cr} may be dominated by fluctuating dipolar fields and at low T by fluctuating contact hyperfine fields.

Clearly our understanding of the two channel relaxation behaviour is rather vague and incomplete. It is an open question to what extent quadrupolar effects are involved, but we can also not exclude them as, at least, the cusp-like anomaly of λ at T_Q demonstrates.

5.3. CeAg

ZF (LF) measurements above T_c extended from 7 K (6) to 300 K (250) [43]. The ZF signal below T_Q displayed a two-component behaviour which was best fitted by the expression

$$P(t) = A_1 \exp(-\lambda_1^* t) + A_2 \exp(-\lambda_2^* t), \tag{5.5}$$

where $\lambda_1^* > \lambda_2^*$ and $A_1/A_2 = 2$ independent of temperature. The fit results for λ_1^*, λ_2^* are displayed in figure 33. Above T_Q the signal is given by a single exponential decay function with relaxation rate λ_0 and amplitude $A_0 = A_1 + A_2 =$ full initial asymmetry. In the range $16\ \text{K} \leqslant T \leqslant 70\ \text{K}$, $\lambda_0(T)$ is excellently fitted by the expression

$$\lambda_0(T) = \frac{\lambda_0}{(T - T^*)^\beta} \tag{5.6}$$

with $\beta = 0.70(4)$ and $T^* = 14.7(4)$ K, which suggests to identify T^* with T_Q (see figure 34). Thus it appears as if $\lambda_0(T)$ reflects a critical slowing down of the Ce 4f-moment as T_Q is approached from above. The fitted critical exponent β agrees with the predictions for a 3D Heisenberg system, with inclusion of non-spin conserving dipole–dipole interactions [75], but this appears rather fortuitous. The slowing down behaviour suggests that the Ce 4f-moments like to enter into a magnetically ordered state already at T_Q. The onset of the quadrupolar order seems to prevent this. Alternatively it is the freezing out of quadrupolar degrees of freedom on approaching T_Q which via the second term in equation (5.1) drives the μ^+ spin relaxation. This would imply that $\tau_Q \ll \tau_{dip}$ and that the contact hyperfine field is the relevant dominating field at the μ^+. According to the Knight shift results the contact fields, averaged over the c sites, are indeed larger than the corresponding dipolar fields.

The two-component behaviour below T_Q with the amplitude ratio 2 and the rather large λ_1^* ($\sim$12 μs^{-1} at 7 K) could suggest that it reflects a static random field distribution of Lorentzian shape and the 1/3-term persisting fluctuating field components perpendicular to the initial

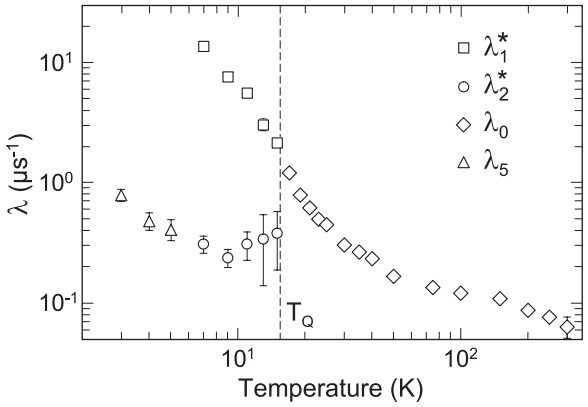

Figure 33. Log–log plot of the temperature dependence of λ_1^* and λ_2^* (equation (5.4)), of λ_0 and λ_5 in CeAg. λ_5 is the relaxation rate of the non-oscillating term below T_c, pointing to fluctuating fields also below T_c (from [43]).

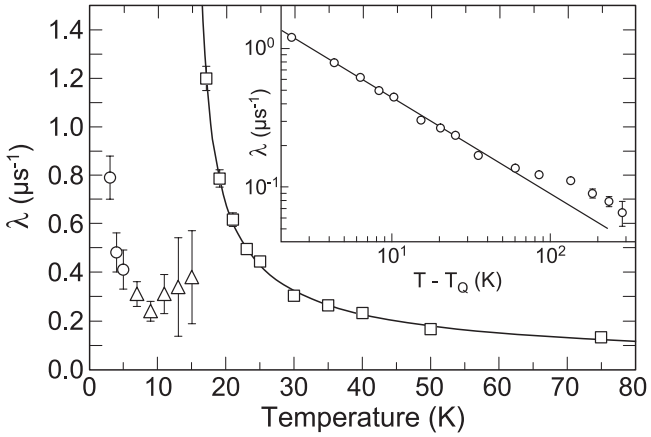

Figure 34. Linear plot of λ_0 in CeAg versus temperature. The solid curve represents a fit of equation (5.5) to the λ_0 data. The inset shows log λ_0 versus log$(T - T_Q)$ (from [43]).

μ^+ polarization. However, λ_1^* is not much reduced in a longitudinal field of 6 kOe (see figure 35), implying that the $2/3$ component in equation (5.4) is not of static origin. Hence both components must be of dynamic origin.

The ratio $A_1/A_2 = 2$ finds a natural explanation if the fluctuations of the Ce 4f-moments are restricted to the tetragonal axes. Suppose that the fluctuations are along the [001] or [010] axes and that the initial μ^+ polarization $\boldsymbol{P}_\mu(0)$ along the [100]-axis. Then μ^+ located at all the d sites will experience fluctuating dipolar and contact fields perpendicular to $\boldsymbol{P}_\mu(0)$ and hence will relax. However, if the fluctuations are restricted to the [100]-axis, parallel to $\boldsymbol{P}_\mu(0)$, the resulting fluctuating fields at the d sites will also be parallel to $\boldsymbol{P}_\mu(0)$, and hence no relaxation will occur. Therefore one expects that $2/3$ of the implanted μ^+ will show relaxation and the remaining $1/3$ fraction no, or only very slow relaxation, perhaps if the sample is slightly misaligned or the fluctuations are not 100% restricted to one of the crystal axes. In any case the onset of ferroquadrupolar order seems to restrict the degrees of freedom of the Ce 4f-moment fluctuations to an uniaxial behaviour. This is not unexpected considering the interdependence of the 4f-quadrupole and magnetic-dipole moments.

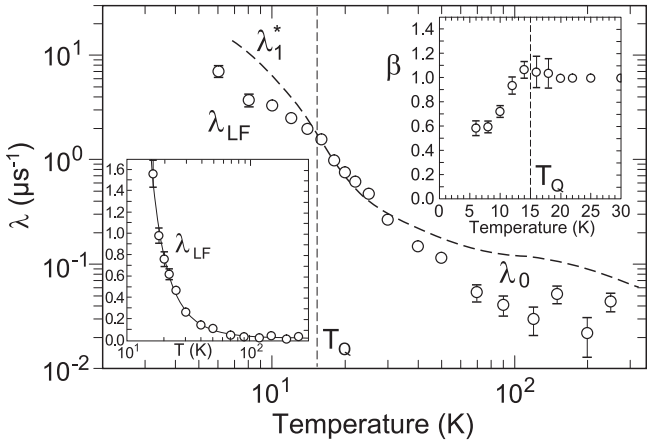

Figure 35. Log–log plot of the LF relaxation rate λ_{LF} in CeAg versus temperature. The ZF relaxation rates λ_1^* and λ_0 are indicated by the dashed line. The inset in the lower left corner displays λ_{LF} versus log T. The solid curve represents again a fit of equation (5.5). The upper right inset displays $\alpha(T)$, see text (from [43]).

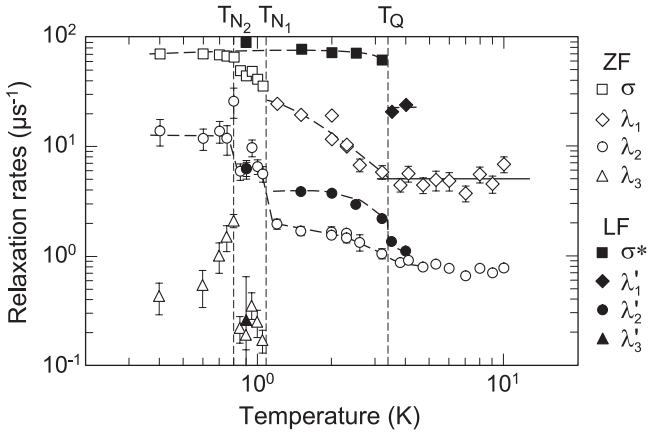

Figure 36. Temperature dependence of the various relaxation rates in $DyPd_3S_4$ in ZF and LF (1 kOe), as defined in equations (4.7)–(4.9). Note the anomalies at T_{N_2}, T_{N_1} and T_Q and the persistence of a Gaussian rate σ in LF above T_{N_1} up to T_Q (from [70]).

Interestingly, in strong longitudinal field the two-component behaviour below T_Q gives way to a one-component stretched exponential behaviour

$$P(t) = A_0 \exp(-(\lambda_{LF} t)^{\alpha}) \tag{5.7}$$

with α approaching 0.5 as T_C is approached from above. Above T_Q $\lambda_{LF}(T)$ is again following equation (5.6), but $T^* \simeq T_C$ and $\beta \simeq 2$. Hence it appears that in LF the slowing down of the Ce 4f-moment dynamics is preparing a freezing at T_C, not at T_Q as in ZF, but the onset of the quadrupolar order disturbs this trend and $\lambda_{LF}(T)$ shows an inflection point at T_Q and not a 'critical' behaviour on approaching T_C. In particular in strong LF the one-dimensional fluctuations below T_Q seem to change to a more isotropic behaviour as above T_Q. The stretched exponential behaviour below T_Q may originate from a spatial distribution of the relaxation rates λ_{LF}, i.e. application of a field introduces a certain inhomogeneity into the system. This feature

has yet to be understood, but it points to competitive mechanisms in the presence of a non-zero H_{ext}. It is, of course, tempting to attribute the different temperature dependences of λ_{ZF} and λ_{LF} above T_Q to the field induced (ferro) quadrupolar state.

In summary, the fluctuating fields at the μ^+, consisting of dipolar and contact hyperfine contributions, are strongly affected by the onset of the ferroquadrupolar order at T_Q. It is possible that the increase of the μ^+ spin relaxation rate on approaching T_Q from above arises from the, perhaps critical, slowing down of quadrupole fluctuations. Below T_Q the fluctuations of the Ce 4f-moments appear to be restricted to the tetragonal crystal axes, along which also the moments are aligned in the ferromagnetic state below T_C.

5.4. $DyPd_3S_4$

As stated in section 4.5, the ZF-μSR signal above $T_{N_1} \simeq 1$ K consists of two exponentially relaxing components [70]. The associated relaxation rates λ_1 and λ_2 are displayed in figure 36. Their temperature dependence shows a clear break at T_Q. The associated amplitudes A_1, A_2 are temperature dependent but $A_1 + A_2 =$ constant = initital asymmetry. This behaviour suggests that the μ^+ reside either in magnetically differently behaving domains or phases or at magnetically/crystallographically inequivalent sites. In any case the populations of the two μ^+ fractions are temperature dependent. Near T_{N_1}, $A_1/A_2 \simeq 4$, which reduces to about 1 above T_Q. λ_1 and λ_2 are interpreted as spin lattice relaxation rates. Hence the onset of antiferroquadrupolar order has a pronounced effect on the Dy 4f-moment dynamics. However, λ_1 and λ_2 are nearly temperature independent above T_Q up at least to 10 K, in contrast to the behaviour in CeAg. The increase of λ_1, λ_2 below T_Q signals a slowing down of the Dy 4f-moment fluctuations inside the quadrupolar ordered phase, but no drastic slowing down upon approaching T_{N_1} is seen. As mentioned in section 4.5, in LF of 6 kOe the amplitudes A_1^* and A_2^* are unchanged from the ZF values, showing the same temperature dependence. However, $\lambda_2^* > \lambda_2$ and the first component changes to a Gaussian behaviour (see figure 36). Hence the Dy 4f-moment dynamics is significantly affected by the applied field: the second component reflects a further reduction of the Dy 4f-moment fluctuation rates below T_Q (but not above T_Q!), and the first component, as mentioned previously, seems even to point to the presence of static magnetic fields at the μ^+. Both features suggested a field induced magnetic order in the antiferroquadrupolar phase below T_Q, which was subsequently confirmed by neutron scattering measurements [70]. By which mechanism the Dy 4f-moment dynamics is controlled by the quadrupolar order is as yet not understood. Measurements on single crystals will shed more light on this problem.

6. Octupolar order in NpO_2?

In connection with the discussion of phase IV in $Ce_{1-x}La_xB_6$ ($x = 0.7, 0.75$) in section 4.3, we mentioned that this phase may be characterized by a ferroquadrupolar order. On the other hand, μSR [61, 62] and NMR [76] studies of phase IV, which revealed some type of magnetic order, suggest that time reversal symmetry is broken in phase IV. This is incompatible with pure quadrupolar order [3]. Hence it was conjectured that octupolar order, which breaks time reversal symmetry, may take place in phase IV and provide a primary order parameter [3, 16]. However, the magnetic fields generated by magnetic octupoles at the μ^+ site are too small to explain the actually measured field spread.

Similar problems are encountered in NpO_2. This compound shows a phase transition at $T_0 \simeq 25.5$ K but neither Mössbauer spectroscopy [77] nor neutron scattering [78] succeeded in finding magnetic order below T_0. In contrast, μSR measurements revealed a spontaneous

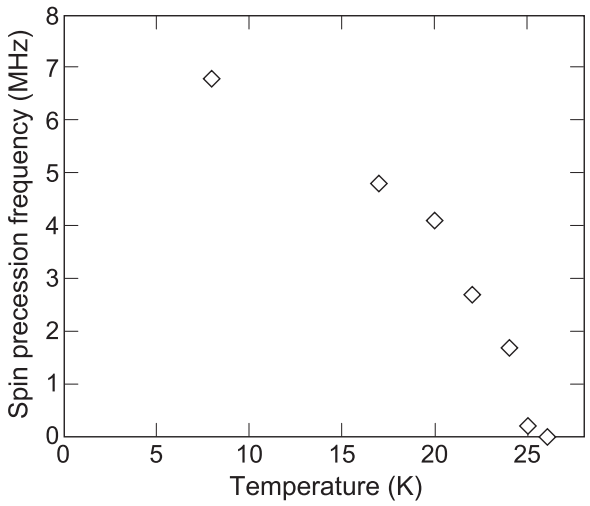

Figure 37. Temperature dependence of the spontaneous precession frequency in NpO_2 (from [79]).

precession signal, appearing below T_0 [79], reflecting an internal field at the μ^+ of $\sim$500 G at 8 K. The temperature dependence of the spontaneous precession frequency is shown in figure 37. The authors of [79] deduce an ordered moment of 0.1 μ_B from the observed internal field. This value is much larger than the upper limit provided by the Mössbauer results: 0.01 μ_B. Results from a resonant x-ray scattering experiment were interpreted to arise from an antiferromagnetic state similar to the one found in UO_2 [80]. However, this interpretation has been questioned in [81]. In any case the small ordered moment extracted from the μSR results is difficult to explain since NpO_2 is a semiconductor and Kondo screening is not possible. As a way out Santini and Amoretti discussed the possibility that NpO_2 develops a magnetic-octupole order below T_0 [4], which would permit the violation of time reversal symmetry and the presence of interstitial magnetic fields. More recently another resonant x-ray experiment by Paixão *et al* [81] revealed directly a long range triple-$\boldsymbol{q}$ antiferroquadrupolar order which could be driven by the ordering of magnetic octupoles below T_0, necessary to explain the μSR and Mössbauer results. Unfortunately, no estimates on the expected interstitial magnetic fields were given and it is questionable whether magnetic octupoles could produce fields of the required strength of 500 G. Such estimates were provided by Kubo and Kuramoto [3] in the case of $Ce_{1-x}La_xB_6$, as discussed in section 4.3, and found to be too small by an order of magnitude compared to the experimental finding. Thus the origin of the spontaneous field at the μ^+ in NpO_2 appears still unsettled and the importance of octupolar effects is an open but most fascinating topic [82].

7. Summary

The information inferred from recent μSR studies, reviewed and elaborated in the previous sections, reflect the richness of physical phenomena provided by the simultaneous presence of different multipole interactions in metallic rare earth and actinide systems. While the interaction of the μ^+ with both the f-shells and conduction electrons is *a priori* magnetic, the orbital exchange mechanism and LS-coupling makes the μSR response of the system to variations of the external parameters $(T, \boldsymbol{B})$ sensitive also to the *orbital* states of the ions.

To clarify this, an expression for the contact interaction parameter A^{con} taking into account orbital exchange scattering in case of CEF-split LSJ levels, has been found and discussed in some detail. One has seen that, in particular, freezing out of quadrupolar degrees of freedom with decreasing temperature, or the reorientation of the quadrupoles following the rotation of the applied field $\boldsymbol{B}$, may be monitored by the variation of A^{con}. In the quadrupolar ordered phase A^{con} may even reflect the temperature dependence of the order parameter, as seems to be observed in CeB_6.

Field induced octupolar ordering is considered to play a decisive role in many cases (e.g. in CeB_6, NpO_2), but it is an open question whether the associated magnetic fields at the μ^+ are strong enough to be noticed.

Beyond the multipolar effects contributing the μ^+ Knight shift, which are in principle understood, unexpected features of possible quadrupolar origin are observed as well. In particular the appearance of a high temperature magnetic order in $PrCu_2$ has to be mentioned. A similar observation is also made in the compound $PrCoAl_4$ (unpublished results). Another feature, indicated by the μSR measurements, is a possible modification of the ordered quadrupolar structure by the onset of magnetic order (e.g. in CeAg, CeB_6 and $PrCu_2$). Not understood at all at present is, in $Ce_{1-x}La_xB_6$ ($x < 0.8$), the observation of short range or random order by μSR and long range order by neutron scattering in the new phase IV. On the other hand, μSR measurements provided the first indication for a field induced antiferromagnetic state in $DyPd_3S_4$ below T_Q, which subsequently was confirmed in more detail by neutron scattering.

Finally, μSR measurements revealed also the influence of quadrupolar effects on the temporal fluctuations of the magnetic fields at the μ^+ site. This may concern the spin dynamics of the f electrons, as in the case of CeAg and $DyPd_3S_4$, or the quadrupolar (and perhaps octupolar) dynamics affecting the contact hyperfine field. An intriguing possibility is that through the μ^+ spin relaxation collective excitations in the quadrupolar ordered state may also become accessible for study.

Acknowledgments

This work could not have been written without the involvement and help of many colleagues in performing the experiments and collecting the data, and providing advice whenever needed. Our thanks extend to F N Gygax, D Andreica, R Feyerherm, M Pinkpank, K A McEwen, Y Ōnuki, S Kunii, O Zaharko, A Tobo, H Onodera, V Pomjakushin, L Keller and Y Kuramoto. Almost all of the work is based on measurement at the Swiss Muon Source at the Paul Scherrer Institute.

References

[1] Morin P and Schmitt D 1990 *Ferromagnetic Materials* (*Handbook of Magnetic Materials* vol 5) ed E P Wohlfarth and K H J Buschow (Amsterdam: Elsevier) p 1
[2] Effantin J M, Rossat-Mignot J, Burlet P, Bartholin H, Kunii S and Kasuya T 1985 *J. Magn. Magn. Mater.* **47/48** 145
[3] Kubo K and Kuramoto Y 2004 *J. Phys. Soc. Japan* **73** 216
[4] Santini P and Amoretti G 2000 *Phys. Rev. Lett.* **85** 2188
[5] Kawarazaki S and Arthur J 1988 *J. Phys. Soc. Japan* **57** 1077
[6] Wun M and Phillip N E 1974 *Phys. Lett.* A **50** 195
Andres K, Darack S and Ott H R 1979 *Phys. Rev.* B **47** 796
[7] Sugiyama K *et al* 1995 *Physica* B **211** 145
[8] Settai R, Araki S, Ahmet P, Abliz M, Sugiyama K, Ōnuki Y, Goto T, Mitamura H, Goto T and Takayanaga S 1998 *J. Phys. Soc. Japan* **67** 636

[9] Zaharko O, Fischer P, Schenck A, Kunii S, Brown P-J, Tasset F and Hansen T 2003 *Phys. Rev.* B **68** 214401
[10] Shiina R, Shiba H and Thalmeier P 1997 *J. Phys. Soc. Japan* **66** 1741
Sakai O, Shiina R, Shiba H and Thalmeier P 1997 *J. Phys. Soc. Japan* **66** 3005
Shiina R, Sakai O, Shiba H and Thalmeier P 1998 *J. Phys. Soc. Japan* **67** 941
[11] Nakao H, Magishi K, Wakabayashi Y, Murakami Y, Koyama K, Hiroto K, Endoh Y and Kunii S 2001 *J. Phys. Soc. Japan* **70** 1857
[12] Kawakami M, Kunii S, Mizuno K, Sugita M, Kasuya T and Kume K 1981 *J. Phys. Soc. Japan* **50** 432
[13] Hiroi M, Sera M, Kobayashi N and Kunii S 1997 *Phys. Rev.* B **55** 8339
[14] Tayama T, Sakakibara T, Tenya K, Amitsuka H and Kunii S 1997 *J. Phys. Soc. Japan* **66** 2268
[15] Iwasa K, Kawakahara K, Kohgi M, Fischer P, Hansen T and Kunii S 2004 at press
[16] Kubo K and Kuramoto Y 2003 *J. Phys. Soc. Japan* **72** 1859
[17] Morin P 1988 *J. Magn. Magn. Mater.* **71** 151
[18] Schmitt D, Morin P and Pierre J 1978 *J. Magn. Magn. Mater.* **8** 249
[19] Onodera H, Yamauchi H and Yamauchi Y 1999 *J. Phys. Soc. Japan* **68** 2526
[20] Onodera H 2004 private communication
[21] Matsuoka E, Kitagawa J, Ohoyama K, Yoshizawa H and Ishikawa M 2001 *J. Phys.: Condens. Matter* **13** 11009
[22] Keller L *et al* 2004 *J. Magn. Magn. Mater. (Proc. ICM'03)* at press
[23] Zochowski S W, de Podesta M, Lester C and McEwen K A 1995 *Physica* B **206/207** 489
[24] Steigenberger U, McEwen K A, Martinez J L and Fort D 1992 *J. Magn. Magn. Mater.* **108** 163
[25] McEwen K A, Steigenberger U, Clausen K N, Kulda J, Park J G and Walker M B 1998 *J. Magn. Magn. Mater.* **177–181** 37
[26] McMorrow P F, McEwen K A, Steigenberger U, Rønnow H M and Yakhou F 2001 *Phys. Rev. Lett.* **87** 057201
[27] McEwen K A, Park J G, Gipson A J and Gehring G A 2003 *J. Phys.: Condens. Matter* **15** 1923
[28] Tokiwa Y *et al* 2000 *Physica* B **281/282** 604
[29] see e.g. Schenck A 1998 *Muon Science* ed C L Lee, S H Kilcoyne and R Cywinski (Bristol: Institute of Physics Publishing)
[30] Sonier J E, Heffner R H, MacLaughlin D E, Nieuwenhuys G J, Bernal O, Movshovich R, Pagliuso P G, Cooley J, Smith J L and Thompson J D 2000 *Phys. Rev. Lett.* **85** 2821
[31] see e.g. McLaughlin D E, Peña O and Lysak M 1981 *Phys. Rev.* B **23** 1039
[32] Feyerherm R, Amato A, Grayevski A, Gygax F N, Kaplan N and Schenck A 1995 *Z. Phys.* B **99** 3
[33] Tashma T, Amato A, Grayevski A, Gygax F N, Pinkpank M, Schenck A and Kaplan N 1997 *Phys. Rev.* B **56** 9397
[34] Gygax F N, Schenck A, Solt G and Canfield P C 2003 *Physica* B **326** 359
[35] Schenck A, Sato N K, Solt G, Andreica D, Gygax F N, Pinkpank M and Amato A 2000 *Eur. Phys. J.* B **13** 245
[36] Schenck A, Gygax F N and McEwen K A 2002 *J. Phys.: Condens. Matter* **14** 4595
[37] see e.g. Schenck A 1981 *Helv. Phys. Acta* **54** 471
[38] De Lorenzi F, Gygax F N, Schenck A, Tobo A and Onodera H 2003 *Physica* B **326** 581
[39] Schenck A, Gygax F N and Kunii S 2002 *Phys. Rev. Lett.* **89** 037201
[40] Saitoh M *et al* 2002 *J. Phys. Soc. Japan* **71** 2369
[41] Givord F, Boucherle J-X, Borlet P, Gillon B and Kunii S 2003 *J. Phys.: Condens. Matter* **15** 3095
[42] Schenck A, Gygax F N, Solt G, Zaharko O and Kunni S 2004 at press
[43] Schenck A, Gygax F N, Andreica D and Ōnuki Y 2003 *J. Phys.: Condens. Matter* **15** 8599
[44] Schenck A, Gygax F N and Ōnuki Y 2003 *Phys. Rev.* B **68** 104422
[45] Gygax F N, Andreica D, Schenck A and Ōnuki Y 2002 *J. Magn. Magn. Mater.* **246** 101
[46] Gygax F N, Andreica D, Schenck A and Ōnuki Y 2004 *J. Phys.: Condens. Matter* **16** 2421
[47] Kittel C 1963 *Quantum Theory of Solids* (New York: Wiley)
[48] Liu S H 1961 *Phys. Rev.* **121** 451
[49] Kaplan T A and Lyons D H 1963 *Phys. Rev.* **129** 2072
[50] Kasuya T and Lyons D H 1966 *J. Phys. Soc. Japan* **21** 287
[51] Coqblin B and Schrieffer J R 1969 *Phys. Rev.* **185** 847
[52] Chan S-K and Lam D J 1974 *The Actinides, Electronic Structure and Related Properties* vol 1, ed A J Freeman and J B Darby (New York: Academic)
[53] Lam D J and Fradin F Y 1974 *Phys. Rev.* B **9** 238
[54] Myers S M and Narath A 1973 *Solid State Commun.* **12** 83
[55] Follstädt D M, Meyer W J and Narath A 1977 *Physica* B **86–88** 507
[56] Dieke G H 1986 *Spectra and Energy Levels of Rare Earth Ions in Crystals* ed H M Crosswhite and H Crosswhite (New York: Interscience)
[57] Siemann R and Cooper B R 1980 *Phys. Rev. Lett.* **44** 1015

[58] Shiba H, Sakai O and Shiina R 1999 *J. Phys. Soc. Japan* **68** 1988
[59] Hanzawa K 2000 *J. Phys. Soc. Japan* **69** 510
[60] see e.g. Kalvius G M, Noakes R D and Hartmann O 2001 *Handbook on the Physics and Chemistry of Rare Earth* vol 32, ed G H Lander, K A Gschneider and Le R Eyring (Amsterdam: Elsevier Science)
[61] Feyerherm R, Amato A, Gygax F N, Schenck A, Ōnuki Y and Sato N 1995 *J. Magn. Magn. Mater.* **140–144** 1175
[62] Takagiwa H, Ohishi K, Akimitsu J, Higemoto W, Kadono R, Sera M and Kunii S 2002 *J. Phys. Soc. Japan* **71** 31
[63] Schenck A *et al* 2003 unpublished
[64] Akatsu M, Goto T, Nemoto Y, Suzuki O, Nakamura S and Kunii S 2003 *J. Phys. Soc. Japan* **72** 205
[65] Kohori Y, Kyogaku M, Kohara T, Asayama K, Amitsuka H and Miyaka Y 1990 *J. Magn. Magn. Mater.* **90/91** 510
[66] de Réotier P D, Yaouanc A, Floquet J, Bonville P, Imbert P, Pari P, Gubbens P C M and Mulders A 1995 *Phys. Lett.* A **205** 239
[67] Aeppli G, Bucher E, Broholm C, Kjems J K, Baumann J and Hufnagel J 1988 *Phys. Rev. Lett.* **60** 615
[68] Isaacs E P, Zschack P, Broholm C L, Buuns C, Aeppli G, Ramirez A P, Palstra T T M, Erwin R W, Stüchli N and Bucher E 1995 *Phys. Rev. Lett.* **75** 1178
[69] Lee M, Moores G F, Song Y Q, Halperin W P, Kim W W and Stewart G R 1993 *Phys. Rev.* B **48** 7392
[70] Keller L, Pomjakushin V, Conder K and Schenck A 2004 *Phys. Rev.* B at press
[71] see e.g. Schlichter C P 1978 *Principle of Magnetic Resonance* (Berlin: Springer)
[72] Kadono R, Higemoto W, Koda A, Kakuta K, Ohishi K, Takagiwa H, Yakoo T and Akimitsu J 2000 *J. Phys. Soc. Japan* **69** 3189
[73] Fukushima N and Kuramoto Y 1998 *J. Phys. Soc. Japan* **67** 2460
[74] Thalmeier P, Shiina R, Shiba H and Sakai O 1998 *J. Phys. Soc. Japan* **67** 2363
[75] see e.g. Yaouanc A, de Réotier P D and Frey E 1993 *Phys. Rev.* B **47** 796
[76] Magishi K, Kawakami M, Saito T, Koyama K, Mizuno K and Kunii S 2002 *Z. Naturf.* a **57** 441
[77] Dunlap B D and Kalvius G M 1985 *Handbook on the Physics and Chemistry of the Actinides* vol 2, ed A J Freeman and G Lander (Amsterdam: North-Holland) p 329
[78] Caciuffo R, Lander G H, Spirlet J G, Fournier J M and Kuhs W F 1987 *Solid State Commun.* **64** 149
[79] Kopmann W *et al* 1998 *J. Alloys Compounds* **271–273** 463
[80] Mannix D, Lander G H, Rebizant J, Caciuffo R, Bernhoeft N, Lidström E and Vettier C 1999 *Phys. Rev.* B **60** 15187
[81] Paixão J A, Detlefs C, Longfield M J, Caciuffo R, Santini P, Bernhoeff N, Rebizant J and Lander G H 2002 *Phys. Rev. Lett.* **89** 187202
[82] Kiss A and Fazekas P 2003 *Phys. Rev.* B **68** 174425
[83] Gavilano J 2004 private communication